frontiers in
IMMUNOLOGY

REVIEW ARTICLE
published: 02 April 2012
doi: 10.3389/fimmu.2012.00065

Alcaligenes is commensal bacteria habituating in the gut-associated lymphoid tissue for the regulation of intestinal IgA responses

Jun Kunisawa[1,2]* and Hiroshi Kiyono[1,2,3,4]*

[1] Division of Mucosal Immunology, Department of Microbiology and Immunology, Institute of Medical Science, The University of Tokyo, Tokyo, Japan
[2] Department of Medical Genome Science, Graduate School of Frontier Science, The University of Tokyo, Tokyo, Japan
[3] Graduate School of Medicine, The University of Tokyo, Tokyo, Japan
[4] Core Research for Evolutional Science and Technology, Japan Science and Technology Agency, Tokyo, Japan

Edited by:
Nils Yngve Lycke, University of Gothenburg, Sweden

Reviewed by:
Paul King, Monash University, Australia
Hiroshi Ohno, RIKEN, Japan

***Correspondence:**
Jun Kunisawa and Hiroshi Kiyono, Division of Mucosal Immunology, Department of Microbiology and Immunology, Institute of Medical Science, The University of Tokyo, Tokyo, Japan.
e-mail: kunisawa@ims.u-tokyo.ac.jp; kiyono@ims.u-tokyo.ac.jp

Secretory-immunoglobulin A (S-IgA) plays an important role in immunological defense in the intestine. It has been known for a long time that microbial stimulation is required for the development and maintenance of intestinal IgA production. Recent advances in genomic technology have made it possible to detect uncultivable commensal bacteria in the intestine and identify key bacteria in the regulation of innate and acquired mucosal immune responses. In this review, we focus on the immunological function of Peyer's patches (PPs), a major gut-associated lymphoid tissue, in the induction of intestinal IgA responses and the unique immunological interaction of PPs with commensal bacteria, especially *Alcaligenes*, a unique indigenous bacteria habituating inside PPs.

Keywords: Peyer's patch, IgA, commensal bacteria

INTRODUCTION

Secretory-immunoglobulin A (S-IgA) is predominantly observed in the intestine where it participates in immune defense (Mestecky et al., 2005; Brandtzaeg, 2010). S-IgA inhibits adherence of pathogens to host epithelial cells in the intestinal lumen and neutralizes pathogenic toxins by binding to the toxins' biologically active sites. Based on the immunological importance of S-IgA in immunosurveillance in the intestine, the development of oral vaccines has focused on the induction of antigen-specific S-IgA responses (Kunisawa et al., 2007). In addition to the immunosurveillance in the intestine, S-IgA antibody contributes to the establishment of beneficial gut commensal microbiota and thus dysfunction of S-IgA formation resulted in the alteration of normal bacterial flora (e.g., the reduction of Lactobacillus and increase of segmented filamentous bacteria, SFB; Suzuki et al., 2004).

Peyer's patches (PPs) are major gut-associated lymphoid tissue (GALT) where intestinal IgA responses are initiated and regulated by unique immunological crosstalk via cytokines [e.g., interleukin-4 (IL-4), IL-6, IL-21, and transforming growth factor-β (TGF-β)] and cell–cell interactions (e.g., via CD40/CD40 ligand interactions) among dendritic, T, and B cells (Kunisawa et al., 2008; Fagarasan et al., 2010). Thus, oral delivery of antigens to PPs is considered an important strategy for the effective induction of antigen-specific intestinal IgA responses (Kunisawa et al., 2011).

In addition to host-derived factors, microbial stimulation is also required for the maximum production of S-IgA in the intestine (Cebra et al., 2005). Indeed, germ-free (GF) mice have decreased intestinal IgA responses with immature structure of GALT when compared with mice housed under SPF or conventional conditions (Weinstein and Cebra, 1991). Although it was reported that some commensal bacteria [e.g., SFB and altered Schaedler flora (ASF), a combined eight culturable bacteria] and bacterial products (e.g., peptidoglycan, CpG oligonucleotide, and LPS) stimulated the intestinal IgA production (Michalek et al., 1983; Talham et al., 1999; Butler et al., 2005), it is obscure which bacteria is involved in this process indigenously. Because predominant commensal bacteria in the intestine is uncultivable, it was difficult to determine by culture-based method which bacteria regulated specific immune responses. However, recent advances in the genomic analysis allowed us to identify the uncultivable bacteria, which revealed key bacteria in the regulation of specific immune responses (Ivanov et al., 2009; Atarashi et al., 2011) as well as the development of immune diseases (Chow et al., 2010; Hill and Artis, 2010). Using genomic and immunological methods, we recently found that the microbial community inside PPs is different from those on the epithelium of PPs or in the intestinal lumen (Obata et al., 2010).

In this review, we discuss initially the immunological features of PPs in the induction and regulation of intestinal IgA responses. In the later part, we focus on the unique cross-communication between PPs and habitat commensal bacteria, *Alcaligenes*, a unique indigenous bacteria habituating inside PPs and regulating dendritic cells (DCs) for the efficient production of intestinal IgA.

IMMUNOLOGICAL FEATURES OF PEYER'S PATCHES

In the intestine, GALT comprise several different, organized lymphoid structures (Spencer et al., 2009; Fagarasan et al., 2010). Among them, PPs are the largest and most well-characterized sites

for the initiation of intestinal IgA responses, especially responses to T cell-dependent antigens (Kunisawa et al., 2008; Fagarasan et al., 2010). There are generally 8–10 PPs in the mouse small intestine and hundreds in the human small intestine. Each PP is composed of several B cell-rich follicles surrounded by a mesh-like structure consisting of T cells known as the interfollicular region (**Figure 1**).

Inside PPs, antigen-sampling M cells located in the follicle-associated epithelium transport luminal antigens to DCs situated in the subepithelium region (Neutra et al., 2001), which then form clusters with T-, B-, and stromal cells in the germinal centers and promote μ-to-α-class-switch recombination of B cells with the help of cytokines such as IL-4, IL-21, and TGF-β (Fagarasan et al., 2010). Upon immunoglobulin class-switching from μ to α, IgA-committed B cells (IgA^+ B cells) begin to express type 1 sphingosine-1-phosphate receptor, CCR9, and α4β7 integrin, allowing them to depart from the PPs and subsequently traffic to the intestinal lamina propria (Mora et al., 2006; Gohda et al., 2008). In the intestinal lamina propria, they further differentiate into IgA-secreting plasma cells under the influence of terminal differentiation factors (e.g., IL-6; Cerutti et al., 2011). DCs play a key role in these processes. For instance, nitric oxide, TGF-β, APRIL, and BAFF produced by TNF-α/iNOS-producing DCs (Tip-DCs) promotes IgA production (Tezuka et al., 2007). Also, DCs in the PPs metabolite vitamin A and produce retinoic acid, which induces the expression of gut-homing receptors (CCR9, and α4β7 integrin) on activated B and T cells (Iwata et al., 2004; Mora et al., 2006). Retinoic acid also induces the preferential differentiation into regulatory T (Treg) cells (Hall et al., 2011), and some of Treg cells differentiated into follicular helper T cells to promote IgA production in the PPs (Tsuji et al., 2009).

The identification of the molecular pathway of PP organogenesis allowed the establishment of PP-deficient mice through the loss of any part of this pathway (Nishikawa et al., 2003). Notably, disruption of the PP organogenesis pathway by blockade of tissue genesis cytokine receptor signaling [IL-7R and/or lymphotoxin-β receptor (LTβR)] during a limited fetus time period results in the selective loss of PPs without affecting other lymphoid tissue organogenesis (Yoshida et al., 1999). Experiments with PP-deficient mice showed that the dependency on PPs in the induction of antigen-specific IgA responses depends on the form of the antigen. For instance, the PP-deficient mice failed to develop antigen-specific IgA responses against orally administered antigens in particle form, but retained their ability to respond to soluble forms of antigens (Yamamoto et al., 2000; Kunisawa et al., 2002). It was also reported that lamina propria DCs are capable of initiating systemic IgG responses, whereas antigen transport by M cells into the PPs is required for the induction of intestinal IgA production (Martinoli et al., 2007). This is consistent with another finding that DCs in the PPs are responsible for intestinal IgA production (Fleeton et al., 2004). Therefore, PPs are considered to be one of the major sites for the initiation of intestinal antigen-specific IgA responses.

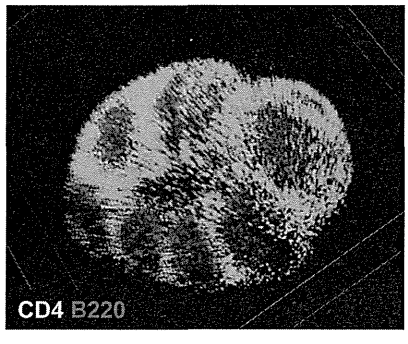

FIGURE 1 | Microarchitecture of murine Peyer's patches. Purified T cells (green) and B cells (red) were chemically labeled with carboxyfluorescein succinimidyl ester and carboxy-SNARF-1, respectively, and adoptively transferred into mice. Fifteen hours after the transfer, cell distribution in the Peyer's patches was observed at the whole-tissue level by using macro-confocal microscopy.

EFFECT OF MICROBIAL STIMULATION ON THE PRODUCTION OF INTESTINAL IgA

It is well known that microbial stimulation is required for the full production of S-IgA in the intestine. Indeed, GF mice have decreased intestinal IgA responses when compared with mice housed under SPF or conventional conditions (Cebra et al., 2005). Studies using mono-associated GF mice with SFB have demonstrated that only a minor proportion of the total intestinal IgA is reactive to mono-associated bacteria (Talham et al., 1999). In addition, bacterial products produced by commonly expressed on commensal bacteria (e.g., peptidoglycan, CpG oligonucleotide, and LPS) stimulated the intestinal IgA production (Michalek et al., 1983; Butler et al., 2005). In contrast, a recent study using reversible colonization of GF mice with genetically engineered *E. coli* showed that intestinal IgA induced in those mice bound to parent strain but not other bacteria (Hapfelmeier et al., 2010). Therefore, it remains unclear whether intestinal IgA responses induced by commensal bacteria is mediated by polyclonal stimulation and/or by B cell receptors specific for microbial antigens.

As one mechanism of impaired IgA production of GF mice, it was reported that GF mice have structurally immature GALT (e.g., PPs and ILFs) when compared with SPF mice (Weinstein and Cebra, 1991; Hamada et al., 2002). In the PPs, several key pathways for the IgA production require microbial stimulation. For example, Tip-DCs enhance the IgA production by producing nitric oxide, TGF-β, APRIL, and BAFF, which requires microbial stimulation through innate receptors (Tezuka et al., 2007). Indeed, the number of Tip-DCs was much reduced in the intestine of GF and MyD88-deficient mice (Tezuka et al., 2007). Another cell involved the microbe-dependent IgA production is non-hematopoietic follicular DCs (FDCs). It was reported that microbial stimulation of FDCs resulted in expressing chemokine CXCL13, BAFF, and TGF-β for the germinal center formation and B cell class-switching from IgM to IgA (Suzuki et al., 2010).

ALCALIGENES IS A UNIQUE INDIGENOUS BACTERIA INSIDE PPs

Recent advances in genomic technology make it possible to detect commensal bacteria in the intestine, allowing identification of key bacteria involved in the regulation of specific immune responses. For example, SFB was identified as commensal bacteria inducing

Th17 cells (Ivanov et al., 2009), whereas colonic regulatory T cells were induced by *Clostridium* clusters IV and XIV (Atarashi et al., 2011). These commensal bacteria localize at the surface of intestinal epithelium, but we supposed that the immunological crosstalk between host and commensal bacteria might establish in the regulation of intestinal IgA responses in the GALT. In this issue, we analyzed the composition of the microbial community inside PPs and identified *Alcaligenes* as a major commensal bacteria uniquely locating inside PPs (Obata et al., 2010).

By using the 16S rRNA clone library method, SFB are the predominant commensal bacteria co-habitat on FAE of PPs as like small intestinal epithelium. Although the FAE consisted with antigen-sampling M cells, SFB was not found inside of PPs. Instead, *Alcaligenes* are predominant bacteria inside PPs. The result obtained by the 16S rRNA analysis was further confirmed by fluorescence *in situ* hybridization (FISH) method and thus *Alcaligenes* are present exclusively inside PPs, not on the FAE of PPs, and intestinal villous epithelium and intestinal lamina propria (**Figure 2**). Of note, the preferential presence of *Alcaligenes* was observed not only in mouse but also in monkey and human (Obata et al., 2010). One of interesting but unresolved questions is the species specificity of *Alcaligenes*. We are now investigating whether *Alcaligenes* isolated from human or monkey colonize in the PPs to promote IgA production when they are orally fed to GF mice. Inside PPs, a proportion of the *Alcaligenes* seemed to be alive in mice. The presence and growth of *Alcaligenes* were detected in the PPs of GF mice after adoptive transfer of PP homogenates containing *Alcaligenes* from SPF mice. These findings suggest that *Alcaligenes* are indigenous bacteria ubiquitously living inside the PPs of various mammalian species.

ANTIBODY-MEDIATED RECIPROCAL INTERACTION BETWEEN *ALCALIGENES* AND THE HOST IMMUNE SYSTEM

As mentioned above, M cells located on the FAE of PPs transport luminal bacteria into DCs locating at the subepithelial region of FAE (Neutra et al., 2001). 16S rRNA clone library methods consistently revealed that DCs in the PPs predominantly contain *Alcaligenes*, whereas these bacteria are rarely detected in DCs isolated from other lymphoid tissues (e.g., spleen and mesenteric lymph nodes; Obata et al., 2010). We examined the immunological effects of *Alcaligenes* on DCs and found that the production of IgA-enhancing cytokines such as IL-6, TGF-β, and BAFF was increased when DCs isolated from the PPs of GF mice were stimulated with *Alcaligenes* (Obata et al., 2010). Several lines of evidence have revealed that immunological functions of DCs are different between intestinal and other lymphoid tissues (reviewed in Rescigno, 2010), we are now investigating whether immune stimulatory functions of *Alcaligenes* is specific for the PP DCs or not.

In agreement with the uptake of *Alcaligenes* and subsequent production of IgA-enhancing cytokines by DCs, *Alcaligenes*-specific IgA-forming cells were frequently observed in PPs, and consequent IgA production was noted in the intestinal lumen of SPF mice, but not GF mice (Obata et al., 2010). Although biological role of *Alcaligenes*-specific IgA antibody remains to be elucidated, the antibody might be involved in the creation of intratissue co-habitation of *Alcaligenes* in PPs. To this end, the number of *Alcaligenes* inside PPs is decreased in B cell-deficient CBA/N xid and IgA-deficient mice compared with wild-type mice (Obata et al., 2010). Therefore, it is interesting to suggest that *Alcaligenes*-specific IgA antibody mediates the uptake and presence of *Alcaligenes* in the PPs. Since M cells express IgA receptors

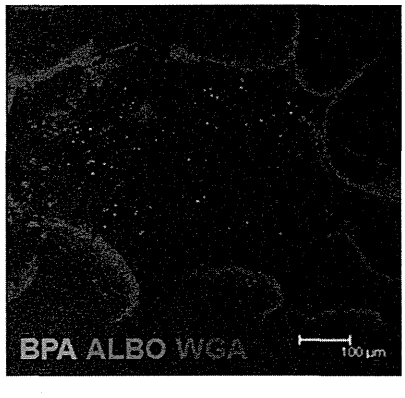

FIGURE 2 | Microarchitecture of murine Peyer's patches. Whole-mount fluorescence *in situ* hybridization was performed to visually analyze the presence of *Alcaligenes* inside PPs. Both BPA and ALBO34a were used as specific probes for *Alcaligenes*. Wheat germ agglutinin (WGA), an *N*-acetylglucosamine-specific lectin, was used to detect epithelial cells. Scale bar indicates 100 μm.

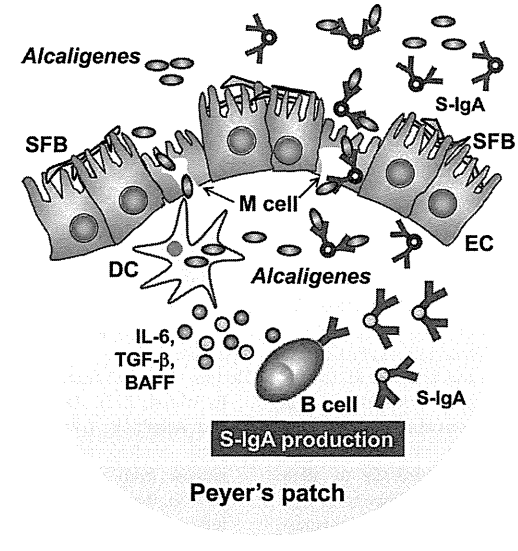

FIGURE 3 | *Alcaligenes* mediates symbiotic communication inside Peyer's patches. On the follicle-associated epithelium of PPs, segmented filamentous bacteria (SFB) is predominantly observed. In contrast, *Alcaligenes* specifically localizes inside Peyer's patches, where some are taken up by dendritic cells (DCs). Stimulation by *Alcaligenes* prompts the DCs to produce IgA-enhancing cytokines [e.g., interleukin-6 (IL-6), transforming growth factor-β (TGF-β)], and B cell activating factor (BAFF), which enhance the intestinal IgA response. The intestinal IgA includes *Alcaligenes*-specific IgA, which might mediate the preferential uptake and presence of *Alcaligenes* in the PPs. The uptake is presumably mediated by M cells.

(Mantis et al., 2002), one possibility is that *Alcaligenes* coated with the *Alcaligenes*-specific antibody are taken up into PPs through M cells. Further, the antigen-specific IgA coating on *Alcaligenes* might be beneficial for the bacteria to create the co-habitation niche since IgA antibody has been shown to non-inflammatory antibody (Mestecky et al., 2005).

CONCLUSION

In this review, we discussed a new concept of symbiotic communication in PPs that is mediated by commensal bacteria-specific IgA antibody. *Alcaligenes*-specific antibodies may mediate the uptake and the presence of *Alcaligenes* in the PPs, and the co-habitation of *Alcaligenes* within the PPs is one of the key factors to promote the intestinal IgA production by enhancing the production of IgA-enhancing cytokines from DCs (**Figure 3**). We still have various questions regarding this co-habitation of *Alcaligenes* in the PPs. For example, it remains unclear whether the presence of *Alcaligenes* inside of PPs is physiologically beneficial or harmful for the host immune system. In this issue, we are now addressing the microbial community in the PPs of mice and human patients suffering from intestinal immune diseases (e.g., intestinal inflammation and allergy). The biological roles of intra-tissue habitation of *Alcaligenes* in the PPs in the appropriate regulation of mucosal immune responses need to be elucidated. The current goal is to elucidate the mechanisms behind the co-habitation of *Alcaligenes* within PPs, and the exact contribution of *Alcaligenes* to educate and guide mucosal immunocompetent cells especially DCs in the PPs for the development, maturation and maintenance of the appropriate host immune system. These studies will provide novel molecular and cellular mechanisms of symbiotic communication with commensal bacteria in the regulation of host immunity.

ACKNOWLEDGMENTS

We thank Dr. T. Obata for his contribution to all works related to *Alcaligenes*, Drs. Y. Benno and M. Sakamoto (RIKEN BioResource Center), and Drs. Y. Umesaki, T. Matsuki, H. Setoyama (Yakult Central Institute for Microbiological Research) for their constructive discussions, technical advice, and supports on microbial analyses, and Dr. H. Iijima (Osaka University) for providing human samples. The work related to this review was supported by grants from the Ministry of Education, Culture, Sports, Science and Technology of Japan [Grant-in-Aid for Young Scientists A (22689015 to Jun Kunisawa), for Scientific Research on Innovative Areas (23116506 to Jun Kunisawa), for Scientific Research S (23229004 to Hiroshi Kiyono), and for Scientific Research on Priority Area (19059003 to Hiroshi Kiyono)]; the Ministry of Health and Welfare of Japan (to Jun Kunisawa and Hiroshi Kiyono); the Global Center of Excellence Program of the Center of Education and Research for Advanced Genome-based Medicine (to Hiroshi Kiyono); the Program for Promotion of Basic and Applied Researches for Innovations in Bio-oriented Industry (to Jun Kunisawa); and the Yakult Bio-Science Foundation (to Jun Kunisawa).

REFERENCES

Atarashi, K., Tanoue, T., Shima, T., Imaoka, A., Kuwahara, T., Momose, Y., Cheng, G., Yamasaki, S., Saito, T., Ohba, Y., Taniguchi, T., Takeda, K., Hori, S., Ivanov, I. I., Umesaki, Y., Itoh, K., and Honda, K. (2011). Induction of colonic regulatory T cells by indigenous *Clostridium* species. *Science* 331, 337–341.

Brandtzaeg, P. (2010). Function of mucosa-associated lymphoid tissue in antibody formation. *Immunol. Invest.* 39, 303–355.

Butler, J. E., Francis, D. H., Freeling, J., Weber, P., and Krieg, A. M. (2005). Antibody repertoire development in fetal and neonatal piglets. IX. Three pathogen-associated molecular patterns act synergistically to allow germfree piglets to respond to type 2 thymus-independent and thymus-dependent antigens. *J. Immunol.* 175, 6772–6785.

Cebra, J. J., Jiang, H. Q., Boiko, N. V., and Tlaskalva-Hogenova, H. (2005). "The role of mucosal microbiota in the development, maintenance, and pathologies of the mucosal immune system," in *Mucosal Immunology*, 3rd Edn, eds J. Mestecky, M. E. Lamm, W. Strober, J. Bienenstock, J. R. Mcghee, and L. Mayer (San Diego: Academic Press), 335–368.

Cerutti, A., Chen, K., and Chorny, A. (2011). Immunoglobulin responses at the mucosal interface. *Annu. Rev. Immunol.* 29, 273–293.

Chow, J., Lee, S. M., Shen, Y., Khosravi, A., and Mazmanian, S. K. (2010). Host-bacterial symbiosis in health and disease. *Adv. Immunol.* 107, 243–274.

Fagarasan, S., Kawamoto, S., Kanagawa, O., and Suzuki, K. (2010). Adaptive immune regulation in the gut: T cell-dependent and T cell-independent IgA synthesis. *Annu. Rev. Immunol.* 28, 243–273.

Fleeton, M. N., Contractor, N., Leon, F., Wetzel, J. D., Dermody, T. S., and Kelsall, B. L. (2004). Peyer's patch dendritic cells process viral antigen from apoptotic epithelial cells in the intestine of reovirus-infected mice. *J. Exp. Med.* 200, 235–245.

Gohda, M., Kunisawa, J., Miura, F., Kagiyama, Y., Kurashima, Y., Higuchi, M., Ishikawa, I., Ogahara, I., and Kiyono, H. (2008). Sphingosine 1-phosphate regulates the egress of IgA plasmablasts from Peyer's patches for intestinal IgA responses. *J. Immunol.* 180, 5335–5343.

Hall, J. A., Grainger, J. R., Spencer, S. P., and Belkaid, Y. (2011). The role of retinoic acid in tolerance and immunity. *Immunity* 35, 13–22.

Hamada, H., Hiroi, T., Nishiyama, Y., Takahashi, H., Masunaga, Y., Hachimura, S., Kaminogawa, S., Takahashi-Iwanaga, H., Iwanaga, T., Kiyono, H., Yamamoto, H., and Ishikawa, H. (2002). Identification of multiple isolated lymphoid follicles on the antimesenteric wall of the mouse small intestine. *J. Immunol.* 168, 57–64.

Hapfelmeier, S., Lawson, M. A., Slack, E., Kirundi, J. K., Stoel, M., Heikenwalder, M., Cahenzli, J., Velykoredko, Y., Balmer, M. L., Endt, K., Geuking, M. B., Curtiss, R. III, Mccoy, K. D., and Macpherson, A. J. (2010). Reversible microbial colonization of germ-free mice reveals the dynamics of IgA immune responses. *Science* 328, 1705–1709.

Hill, D. A., and Artis, D. (2010). Intestinal bacteria and the regulation of immune cell homeostasis. *Annu. Rev. Immunol.* 28, 623–667.

Ivanov, I. I., Atarashi, K., Manel, N., Brodie, E. L., Shima, T., Karaoz, U., Wei, D., Goldfarb, K. C., Santee, C. A., Lynch, S. V., Tanoue, T., Imaoka, A., Itoh, K., Takeda, K., Umesaki, Y., Honda, K., and Littman, D. R. (2009). Induction of intestinal Th17 cells by segmented filamentous bacteria. *Cell* 139, 485–498.

Iwata, M., Hirakiyama, A., Eshima, Y., Kagechika, H., Kato, C., and Song, S. Y. (2004). Retinoic acid imprints gut-homing specificity on T cells. *Immunity* 21, 527–538.

Kunisawa, J., Kurashima, Y., and Kiyono, H. (2011). Gut-associated lymphoid tissues for the development of oral vaccines. *Adv. Drug Deliv. Rev.* [Epub ahead of print].

Kunisawa, J., Mcghee, J., and Kiyono, H. (2007). "Mucosal S-IgA enhancement: development of safe and effective mucosal adjuvants and mucosal antigen delivery vehicles," in *Mucosal Immune Defense: Immunoglobulin A*, ed. C. Kaetzel (New York: Kluwer Academic/Plenum Publishers), 346–389.

Kunisawa, J., Nochi, T., and Kiyono, H. (2008). Immunological commonalities and distinctions between airway and digestive immunity. *Trends Immunol.* 29, 505–513.

Kunisawa, J., Takahashi, I., Okudaira, A., Hiroi, T., Katayama, K., Ariyama, T., Tsutsumi, Y., Nakagawa, S., Kiyono, H., and Mayumi, T. (2002). Lack of antigen-specific immune responses in anti-IL-7 receptor α chain antibody-treated Peyer's patch-null mice following intestinal immunization with microencapsulated antigen. *Eur. J. Immunol.* 32, 2347–2355.

Mantis, N. J., Cheung, M. C., Chintalacharuvu, K. R., Rey, J., Corthesy, B., and Neutra, M. R. (2002). Selective adherence of IgA to murine Peyer's patch M cells: evidence for a novel IgA receptor. *J. Immunol.* 169, 1844–1851.

Martinoli, C., Chiavelli, A., and Rescigno, M. (2007). Entry route of *Salmonella typhimurium* directs the type of induced immune response. *Immunity* 27, 975–984.

Mestecky, J., Moro, I., Kerr, M. A., and Woof, J. M. (2005). "Mucosal immunoglobulins," in *Mucosal Immunology*, 3rd Edn, eds J. Mestecky, M. E. Lamm, W. Strober, J. Bienenstock, J. R. Mcghee, and L. Mayer (San Diego: Academic Press), 153–182.

Michalek, S. M., Morisaki, I., Gregory, R. L., Kiyono, H., Hamada, S., and Mcghee, J. R. (1983). Oral adjuvants enhance IgA responses to *Streptococcus mutans*. *Mol. Immunol.* 20, 1009–1018.

Mora, J. R., Iwata, M., Eksteen, B., Song, S. Y., Junt, T., Senman, B., Otipoby, K. L., Yokota, A., Takeuchi, H., Ricciardi-Castagnoli, P., Rajewsky, K., Adams, D. H., and Von Andrian, U. H. (2006). Generation of gut-homing IgA-secreting B cells by intestinal dendritic cells. *Science* 314, 1157–1160.

Neutra, M. R., Mantis, N. J., and Kraehenbuhl, J. P. (2001). Collaboration of epithelial cells with organized mucosal lymphoid tissues. *Nat. Immunol.* 2, 1004–1009.

Nishikawa, S., Honda, K., Vieira, P., and Yoshida, H. (2003). Organogenesis of peripheral lymphoid organs. *Immunol. Rev.* 195, 72–80.

Obata, T., Goto, Y., Kunisawa, J., Sato, S., Sakamoto, M., Setoyama, H., Matsuki, T., Nonaka, K., Shibata, N., Gohda, M., Kagiyama, Y., Nochi, T., Yuki, Y., Fukuyama, Y., Mukai, A., Shinzaki, S., Fujihashi, K., Sasakawa, C., Iijima, H., Goto, M., Umesaki, Y., Benno, Y., and Kiyono, H. (2010). Indigenous opportunistic bacteria inhabit mammalian gut-associated lymphoid tissues and share a mucosal antibody-mediated symbiosis. *Proc. Natl. Acad. Sci. U.S.A.* 107, 7419–7424.

Rescigno, M. (2010). Intestinal dendritic cells. *Adv. Immunol.* 107, 109–138.

Spencer, J., Barone, F., and Dunn-Walters, D. (2009). Generation of immunoglobulin diversity in human gut-associated lymphoid tissue. *Semin. Immunol.* 21, 139–146.

Suzuki, K., Maruya, M., Kawamoto, S., Sitnik, K., Kitamura, H., Agace, W. W., and Fagarasan, S. (2010). The sensing of environmental stimuli by follicular dendritic cells promotes immunoglobulin A generation in the gut. *Immunity* 33, 71–83.

Suzuki, K., Meek, B., Doi, Y., Muramatsu, M., Chiba, T., Honjo, T., and Fagarasan, S. (2004). Aberrant expansion of segmented filamentous bacteria in IgA-deficient gut. *Proc. Natl. Acad. Sci. U.S.A.* 101, 1981–1986.

Talham, G. L., Jiang, H. Q., Bos, N. A., and Cebra, J. J. (1999). Segmented filamentous bacteria are potent stimuli of a physiologically normal state of the murine gut mucosal immune system. *Infect. Immun.* 67, 1992–2000.

Tezuka, H., Abe, Y., Iwata, M., Takeuchi, H., Ishikawa, H., Matsushita, M., Shiohara, T., Akira, S., and Ohteki, T. (2007). Regulation of IgA production by naturally occurring TNF/iNOS-producing dendritic cells. *Nature* 448, 929–933.

Tsuji, M., Komatsu, N., Kawamoto, S., Suzuki, K., Kanagawa, O., Honjo, T., Hori, S., and Fagarasan, S. (2009). Preferential generation of follicular B helper T cells from Foxp3+ T cells in gut Peyer's patches. *Science* 323, 1488–1492.

Weinstein, P. D., and Cebra, J. J. (1991). The preference for switching to IgA expression by Peyer's patch germinal center B cells is likely due to the intrinsic influence of their microenvironment. *J. Immunol.* 147, 4126–4135.

Yamamoto, M., Rennert, P., Mcghee, J. R., Kweon, M. N., Yamamoto, S., Dohi, T., Otake, S., Bluethmann, H., Fujihashi, K., and Kiyono, H. (2000). Alternate mucosal immune system: organized Peyer's patches are not required for IgA responses in the gastrointestinal tract. *J. Immunol.* 164, 5184–5191.

Yoshida, H., Honda, K., Shinkura, R., Adachi, S., Nishikawa, S., Maki, K., Ikuta, K., and Nishikawa, S. I. (1999). IL-7 receptor α^+ CD3- cells in the embryonic intestine induces the organizing center of Peyer's patches. *Int. Immunol.* 11, 643–655.

Conflict of Interest Statement: The authors declare that the research was conducted in the absence of any commercial or financial relationships that could be construed as a potential conflict of interest.

Received: 27 January 2012; paper pending published: 15 February 2012; accepted: 15 March 2012; published online: 02 April 2012.

Citation: Kunisawa J and Kiyono H (2012) Alcaligenes is commensal bacteria habituating in the gut-associated lymphoid tissue for the regulation of intestinal IgA responses. Front. Immun. 3:65. doi: 10.3389/fimmu.2012.00065

This article was submitted to Frontiers in Mucosal Immunity, a specialty of Frontiers in Immunology.

The Airway Antigen Sampling System: Respiratory M Cells as an Alternative Gateway for Inhaled Antigens

Dong-Young Kim,[*,†,1] Ayuko Sato,[*,1] Satoshi Fukuyama,[*,1] Hiroshi Sagara,[‡] Takahiro Nagatake,[*,§] Il Gyu Kong,[*,†,§] Kaoru Goda,[*] Tomonori Nochi,[*] Jun Kunisawa,[*,¶] Shintaro Sato,[*] Yoshifumi Yokota,[‖] Chul Hee Lee,[†] and Hiroshi Kiyono[*,§,¶,#,]**

In this study, we demonstrated a new airway Ag sampling site by analyzing tissue sections of the murine nasal passages. We revealed the presence of respiratory M cells, which had the ability to take up OVA and recombinant *Salmonella typhimurium* expressing GFP, in the turbinates covered with single-layer epithelium. These M cells were also capable of taking up respiratory pathogen group A *Streptococcus* after nasal challenge. Inhibitor of DNA binding/differentiation 2 (Id2)-deficient mice, which are deficient in lymphoid tissues, including nasopharynx-associated lymphoid tissue, had a similar frequency of M cell clusters in their nasal epithelia to that of their littermates, $Id2^{+/-}$ mice. The titers of Ag-specific Abs were as high in $Id2^{-/-}$ mice as in $Id2^{+/-}$ mice after nasal immunization with recombinant *Salmonella*-ToxC or group A *Streptococcus*, indicating that respiratory M cells were capable of sampling inhaled bacterial Ag to initiate an Ag-specific immune response. Taken together, these findings suggest that respiratory M cells act as a nasopharynx-associated lymphoid tissue-independent alternative gateway for Ag sampling and subsequent induction of Ag-specific immune responses in the upper respiratory tract. *The Journal of Immunology*, **2011, 186: 4253–4262.**

The initiation of Ag-specific immune responses occurs at special gateways, M cells, which are located in the epithelium overlying MALT follicles such as nasopharynx-associated lymphoid tissue (NALT) and Peyer's patches (1). Peyer's patches contain all of the immunocompetent cells that are required for the generation of an immune response and are the key inductive tissues for the mucosal immune system. Peyer's patches are interconnected with effector tissues (e.g., the lamina propria of the intestine) for the induction of IgA immune responses specific to ingested Ags (2). NALT also contains all of the necessary lymphoid cells, including T cells, B cells, and APCs, for the induction and regulation of inhaled Ag-specific mucosal immune responses (1, 3). This tissue is rich in Th0-type $CD4^+$ T cells, which can become either Th1- or Th2-type cells (4). NALT is also equipped with the molecular and cellular environments for class-switch recombination of μ to α genes for the generation of IgA-committed B cells and the induction of memory B cells (5, 6). It is thus widely accepted that NALT M cells are key players in the uptake of nasally delivered Ags for the subsequent induction of Ag-specific IgA immune responses (1). As a result, NALT is considered a potent target for mucosal vaccines (1).

A recent study identified NALT-like structures of lymphocyte aggregates with follicle formation in the human nasal mucosa, especially in the middle turbinate of children <2 y old (7). Another recent study showed that, postinfection of mice with influenza via the upper respiratory tract, the levels of Ag-specific Ig observed in the serum and in nasal mucosal secretions after surgical removal of NALT were comparable to those in tissue-intact mice (8). Other studies have demonstrated that Ag-specific immune responses are induced in lymphotoxin-$\alpha^{-/-}$ and $CXCL13^{-/-}$ mice, in which the NALT exhibits structural and functional defects (9, 10). Thus, despite the central role of NALT in the generation of Ag-specific Th cells and IgA-committed B cells against inhaled Ags, these tissues do not appear essential for the induction of Ag-specific immune responses, suggesting that additional inductive sites and/or M cells are present in the upper respiratory tract.

The major goal of our study was to search for an NALT-independent M cell-operated gateway by examining and characterizing the entire nasal mucosa. We were able to identify M cells developed in the murine nasal passage epithelium as an alternative and NALT-independent gateway for the sampling of respiratory Ags and the subsequent induction of Ag-specific immune

*Division of Mucosal Immunology, Department of Microbiology and Immunology, Institute of Medical Science, University of Tokyo, Tokyo 108-8639, Japan; †Department of Otorhinolaryngology, Seoul National University College of Medicine, Seoul 110-744, Korea; ‡Medical Proteomics Laboratory, Institute of Medical Science, University of Tokyo, Tokyo 108-8639, Japan; §Graduate School of Medicine and Faculty of Medicine, University of Tokyo, Tokyo 113-0033, Japan; ¶Graduate School of Frontier Sciences, University of Tokyo, Chiba 277-8561, Japan; ‖Department of Molecular Genetics, School of Medicine, University of Fukui, Fukui 910-1193, Japan; #Immunobiology Vaccine Center, University of Alabama at Birmingham, Birmingham, AL 35294; and **Department of Pediatric Dentistry, University of Alabama at Birmingham, Birmingham, AL 35294

[1]D.-Y.K., A.S., and S.F contributed equally to this work.

Received for publication November 25, 2009. Accepted for publication February 2, 2011.

This work was supported by grants-in-aid from the Ministry of Education, Science, Sports, and Culture and the Ministry of Health and Welfare of Japan. Part of the study was also supported by grants from the Joint Research Project under the Korea–Japan Basic Scientific Cooperation Program for FY 2007, Seoul National University Hospital Research Fund 05-2007-004, and the Waksman Foundation. D.-Y.K. was supported by research fellowships from the Japan Society for the Promotion of Science for Foreign Researchers. S.F., T.N., and T.N. were supported by research fellowships from the Japan Society for the Promotion of Science for Young Scientists.

Address correspondence and reprint requests to Dr. Hiroshi Kiyono, Division of Mucosal Immunology, Department of Microbiology and Immunology, Institute of Medical Science, University of Tokyo, 4-6-1 Shirokanedai, Minato-ku, Tokyo 108-8639, Japan. E-mail address: kiyono@ims.u-tokyo.ac.jp

The online version of this article contains supplemental material.

Abbreviations used in this article: DC, dendritic cell; dLN, draining lymph node; GAS, group A *Streptococcus*; GFP-*Salmonella*, GFP-expressing *Salmonella*; Id2, inhibitor of DNA binding/differentiation 2; NALT, nasopharynx-associated lymphoid tissue; *Salmonella*-GFP, *Salmonella typhimurium* expressing GFP; SEM, scanning electron microscopy; TEM, transmission electron microscopy; TT, tetanus toxoid; UEA-1, *Ulex europaeus* agglutinin-1; WGA, wheat germ agglutinin.

www.jimmunol.org/cgi/doi/10.4049/jimmunol.0903794

responses. Characterization of respiratory M cells should accelerate our understanding of the Ag sampling system at work in the upper respiratory tract.

Materials and Methods

Mice

BALB/c mice were purchased from SLC (Shizuoka, Japan). Inhibitor of DNA binding/differentiation 2 (Id2)$^{-/-}$ mice (129/Sv), generated as previously described (11), were maintained together with their littermate Id2$^{+/-}$ mice in a specific pathogen-free environment at the experimental animal facility of the Institute of Medical Science, University of Tokyo. All experiments were carried out according to the guidelines provided by the Animal Care and Use Committees of the University of Tokyo.

M cell staining

For the preparation of nasal cavity samples for confocal microscopy, we decapitated euthanized mice and then, with their heads immobilized, removed the lower jaw together with the tongue. Using the hard palate as a guide, we then used a large scalpel to remove the snout with a transverse cut behind the back molars. After removing the skin and any excess soft tissue, we flushed the external nares with PBS to wash out any blood within the nasal cavity before freezing the nasal passage tissue in Tissue-Tek OCT embedding medium (Miles, Elkhart, IN) in a Tissue-Tek Cryomold. For immunofluorescence staining, we prepared 5-μm–thick frozen sections by using a CryoJane Tape-Transfer System (Instrumedics, St. Louis, MO), allowed the sections to air dry, and then fixed them in acetone at 4°C. We then rehydrated the sections in PBS and incubated them for a further 30 min in Fc blocking solution. For M cell staining, sections were incubated overnight with rhodamine-labeled *Ulex europaeus* agglutinin-1 (UEA-1; Vector Laboratories, Burlingame, CA) at a concentration of 20 μg/ml and FITC-labeled M cell-specific mAb NKM 16-2-4 (12) at 5 μg/ml or FITC-labeled wheat germ agglutinin (WGA; Vector Laboratories, Burlingame, CA) at 10 μg/ml and counterstained with DAPI (Molecular Probes, Eugene, OR) at 0.2 μg/ml in PBS (13).

Electron microscopic analysis of respiratory M cells

For electron microscopic analysis, the nasal cavity sample was prepared and vigorously washed as described above, and then fixed on ice for 1 h in a solution containing 0.5% glutaraldehyde, 4% paraformaldehyde, and 0.1 M sodium phosphate buffer (pH 7.6). After being washed with 4% sucrose in 0.1 M phosphate buffer, the tissues were incubated in an HRP-conjugated UEA-1 solution (20 μg/ml) for 1 h at room temperature. The peroxidase reaction was developed by incubating the tissues for 10 min at room temperature with 0.02% 3,3′-diaminobenzidine tetrahydrochloride in 0.05 M Tris-HCl (pH 8) containing 0.01% H_2O_2. After being washed with the same buffer, the tissues were fixed again with 2.5% glutaraldehyde in 0.1 M phosphate buffer overnight. The nasal passage tissue was decalcified with 2.5% EDTA solution for 5 d. After being washed three times with the same buffer, samples were fixed with 2% osmium tetraoxide on ice for 1 h before being dehydrated with a series of ethanol gradients. For scanning electron microscopy (SEM), dehydrated tissues were freeze-embedded in *t*-butyl alcohol and freeze-dried, then coated with osmium and observed with a Hitachi S-4200 scanning electron microscope (Hitachi, Tokyo, Japan). For transmission electron microscopy (TEM) analysis, the samples were embedded in Epon 812 Resin mixture (TAAB Laboratories Equipment, Berks, U.K.), and ultrathin (70-nm) sections were cut with a Reichert Ultracut N Ultramicrotome (Leica Microsystems, Heidelberg, Germany). Ultrathin sections were stained with 2% uranyl acetate in 70% ethanol for 5 min at room temperature and then in Reynolds lead citrate for 5 min at room temperature. Sections were examined with a Hitachi H-7500 transmission electron microscope (Hitachi, Tokyo, Japan).

Elucidation of M cell numbers

To examine the numbers of respiratory and NALT M cells, mononuclear cells (including M cells, epithelial cells, and lymphocytes) were isolated from the nasal passages and NALT as previously described, with some modifications (4). In brief, the palatine plate containing NALT was removed, and then NALT was dissected out. Nasal passage tissues without NALT were also extracted from the nasal cavity, and mononuclear cells from individual tissues were isolated by gentle teasing using needles through 40-μm nylon mesh. The total numbers of cells isolated from the two preparations were counted. These single-cell preparations were then labeled with PE–UEA-1 (Biogenesis, Poole, England), and the percentages of UEA-1–positive epithelial cells in the nasal passages and NALT were determined with a flow cytometer (FACSCalibur; BD Biosciences, Franklin Lakes, NJ). The numbers of M cells and goblet cells in the nasal passages and NALT were counted by confocal microscopic analysis according to the patterns of staining with UEA-1 and WGA. That is, the frequencies of M cells (UEA-1$^+$WGA$^-$) and goblet cells (UEA-1$^+$WGA$^+$) were determined by the enumeration of each type in 100 UEA-1$^+$ cells. The formula used to estimate the number of M cells was: [(total number of mononuclear cells × percentage of UEA-1$^+$ epithelial cells) × M cells/UEA-1$^+$ epithelial cells]. The number of respiratory M cells in Id2$^{-/-}$ mice was calculated in the same manner.

Ag uptake in situ

DQ OVA was purchased from Molecular Probes. *Salmonella typhimurium* PhoPc strain transformed with the pKKGFP plasmid was kindly provided by F. Niedergang (14, 15). Group A *Streptococcus* (GAS; *Streptococcus pyogenes* ATCC BAA-1064) was obtained from the American Type Culture Collection (Manassas, VA), and immunofluorescence staining with FITC-conjugated goat anti-*Streptococcus* A Ab (Cortex Biochem, San Leandro, CA) was used to detect GAS uptake. DQ OVA (0.5 mg), GFP-expressing *Salmonella* (GFP-*Salmonella*) (5 × 10^8 CFU), or GAS (5 × 10^8 CFU) was intranasally administered and incubated in situ. Thirty minutes after the intranasal administration, the nasal passages were removed as described above and extensively washed with cold PBS with antibiotic solution to remove weakly adherent and/or extracellular DQ OVA or bacteria, as described (13).

The airway fluorescence-labeled Ag-treated nasal passages were processed for confocal microscopy as described above or for FACSCalibur flow cytometric analysis as follows. Mononuclear cells (including M cells, epithelial cells, and lymphocytes) were physically isolated from the nasal passages and NALT as described above, fixed in 4% paraformaldehyde, and labeled with PE–UEA-1 (Biogenesis, Poole, England). The percentage of green fluorescence (BODYPI FL or GFP)/UEA-1 double-positive nasal passage epithelial cells was determined by using an FACSCalibur (BD Biosciences).

To clarify the uptake of the bacteria by M cells, UEA-1$^+$GFP$^+$ cells, which were sorted from the nasal passages of mice intranasally infected with GFP-*Salmonella* by using an FACSAria cell sorter (BD Biosciences) were analyzed under three-dimensional confocal microscopy (Leica Microsystems).

To demonstrate the presence of dendritic cells (DCs) in the submucosa of the nasal passages, especially underneath respiratory M cells, after intranasal instillation of GAS, we used FITC- or allophycocyanin-conjugated anti-mouse CD11c (BD Pharmingen, San Jose, CA) Abs for subsequent confocal microscopic analysis.

Immunization

The recombinant *S. typhimurium* BRD 847 strain used in this study was a double *aroA aroD* mutant that expressed the nontoxic, immunogenic 50-kDa ToxC fragment of tetanus toxin from the plasmid pTET*nir*15 under the control of the anaerobically inducible *nirB* promoter (recombinant *Salmonella*-ToxC) (16). As a control, recombinant *Salmonella* that did not express ToxC was used. The recombinant *Salmonella* organisms were resuspended in PBS to a concentration of 2.5 × 10^{10} CFU/ml. Bacterial suspensions were intranasally administered by pipette (10 μl/mouse) three times at weekly intervals. To eliminate any possible GALT-associated induction of Ag-specific immune responses from the swallowing of bacterial solutions after intranasal immunization, mice were given drinking water containing gentamicin from 1 wk before the immunization to the end of the experiment and were also subjected to intragastric lavage with 500 μl gentamicin solution before and after intranasal immunization. This protocol successfully eliminated the possibility of the intranasally delivered bacteria becoming deposition in the intestine (Supplemental Fig. 1). The titers of tetanus toxoid (TT)-specific serum IgG and mucosal IgA Abs were determined by end-point ELISA, as described previously (17).

To measure GAS-specific immune responses, GAS was suspended in PBS to a concentration of 2 × 10^{10} CFU/ml. Ten microliters bacterial suspension was intranasally administered once using a pipette. Six weeks after the administration, serum and nasal washes were prepared, and the titers of GAS-specific Ab were measured by ELISA using a previously described protocol (18).

Statistical analysis

Data are expressed as means ± SD, and the difference between groups was assessed by the Mann–Whitney *U* test. The p values <0.05 were considered to be statistically significant.

Results

Respiratory M cells in single-layer epithelium of the nasal passage

The nasal respiratory epithelium of the mouse is composed mainly of pseudostratified ciliated columnar epithelium (19). However, when H&E-stained sections of the whole nasal cavity were examined, a single-layer epithelium was found to cover some regions of the nasal cavity, especially the lateral surfaces of the nasal turbinates (Fig. 1*A–C*). Frozen sections of nasal passages from naive BALB/c mice were prepared and stained with FITC-WGA (green) and rhodamine–UEA-1 (red), and then counterstained with DAPI (blue). Clusters of UEA-1$^+$WGA$^-$ cells that shared M cell characteristics were found exclusively in the single-layer epithelium of the nasal passage covered by ciliated columnar epithelial cells (Fig. 1*D*, 1*E*). Some respiratory M cells were also occasionally found on the transitional area between the single-layer and stratified epithelium. Notably, respiratory M cells also reacted with our previously developed M cell-specific mAb NKM 16-2-4 (12), demonstrating colocalization of the signals of UEA-1 and NKM 16-2-4 (Fig. 1*F*, 1*G*).

Electron microscopic analysis of respiratory M cells

SEM of the respiratory M cells revealed the characteristic features of M cells: a depressed surface with short and irregular microvilli (Fig. 2*A*, 2*B*). TEM analysis revealed that the respiratory M cell was covered by shorter and more irregular microvilli (with definite UEA-1$^+$ signals; Fig. 2*C*, 2*D*) than were found in neighboring ciliated columnar respiratory epithelial cells (Fig. 2*E*). However, no pocket formation (or pocket lymphocytes) was seen in the basal membranes of respiratory M cells, unlike in NALT M cells (Fig. 2*F*, 2*G*). These findings indicated that the newly identified respiratory M cells had most of the unique morphological characteristics of classical M cells.

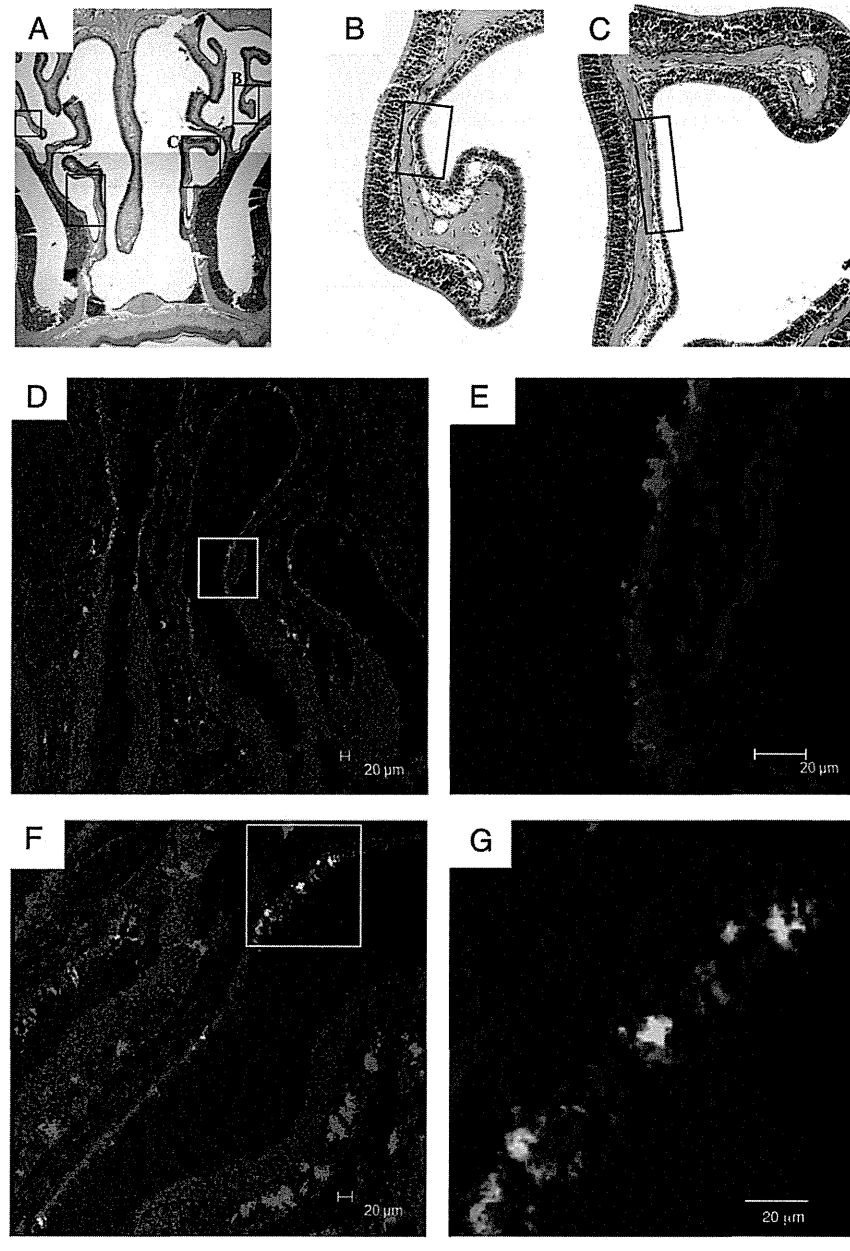

FIGURE 1. Clusters of UEA-1$^+$WGA$^-$ respiratory M cells are found selectively in the single-layer epithelium of the nasal passage. *A–C*, H&E staining reveals the anatomy and general histology of the murine nasal passage (*A*, original magnification ×40). The nasal respiratory epithelium of the mouse is covered with a pseudostratified ciliated columnar epithelium. However, a single-layer epithelium was found on the lateral surfaces of the nasal turbinates (*B*, *C*). Original magnification ×100. Rectangles indicate areas covered with the single-layer epithelium. The results are representative of three independent experiments. *D–G*, Confocal views of UEA-1$^+$ cells in the nasal epithelium of turbinates. Frozen sections were prepared and stained with FITC-WGA (green) and rhodamine–UEA-1 (red), and then counterstained with DAPI (blue) (*D*, *E*). Scale bars, 20 μm. The merged image is shown in *D*. An enlargement of the area in the rectangle in *D* is shown in *E*. UEA-1$^+$WGA$^-$ cells are clustered on the single-layer nasal epithelium of the turbinate. *F* and *G*, UEA-1$^+$ cells also reacted with our previously developed M cell-specific mAb NKM 16-2-4, demonstrating colocalization of signals of rhodamine–UEA-1 (red) and FITC-NKM 16-2-4 (green). The merged image is shown in *F*. An enlargement of an area from the rectangle in *F* is shown in *G*. The results are representative of five independent experiments.

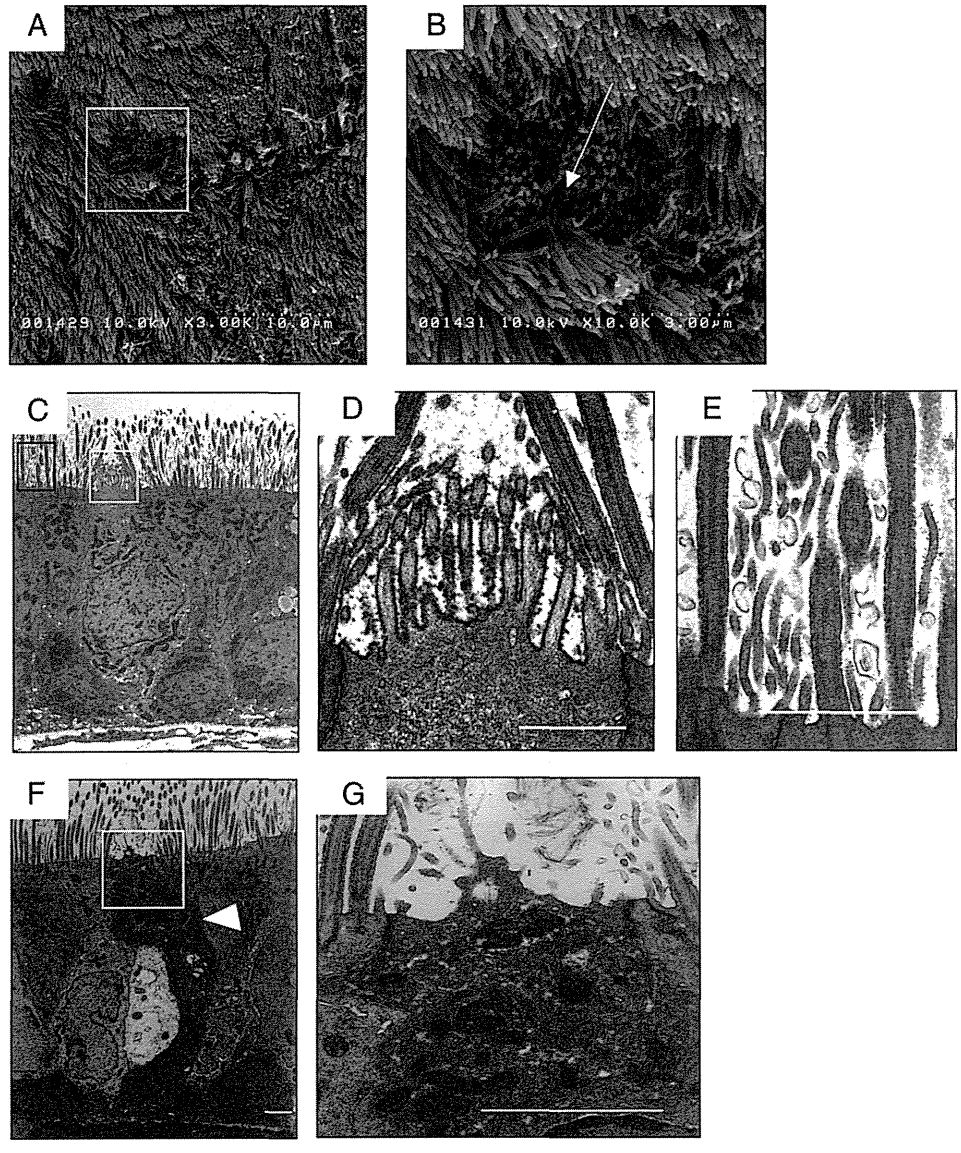

FIGURE 2. Electron microscopic analysis of respiratory M cells. *A* and *B*, SEM analysis shows that the M cells (*B*, arrow) in the nasal passage epithelium are distinguishable from adjacent respiratory epithelial cells by their relatively depressed and dark brush borders. An enlargement of the area in the rectangle in *A* is shown in *B*. As indicated in the *Materials and Methods*, the tissue specimen was incubated with HRP-conjugated UEA-1 before TEM analysis. *C–E*, TEM analysis of respiratory M cells reveals shorter and more irregular microvilli with definite UEA-1$^+$ signals (*D*), unlike the cilia of neighboring respiratory epithelial cells (*E*). *F* and *G*, TEM analysis of NALT M cells. A readily apparent intraepithelial pocket with mononuclear cells (*F*, arrowhead) and short microvilli on the apical surfaces of NALT M cells are seen. The white squares in *C* and *F* indicate UEA-1$^+$ respiratory and NALT M cells, respectively, and are magnified in *D* and *G*, respectively. The black rectangle in *C* indicates an adjacent respiratory epithelial cell and is magnified in *E*. *C–G*, Scale bars, 0.5 μm. Results are representative of four independent experiments.

Protein and bacterial Ag uptake by respiratory M cells

Because M cells were frequently found in the single layer of nasal passage epithelium (Fig. 1*D–G*), we next examined the ability of respiratory M cells to take up various forms of Ag from the lumen of the nasal cavity. DQ OVA or recombinant *Salmonella typhimurium* expressing GFP (*Salmonella*-GFP) was instilled into the nasal cavities of BALB/c mice via the nares. Thirty minutes after the intranasal instillation, immunohistological analyses revealed that the M cells located on the lateral surfaces of the nasal turbinates in the single layer of nasal epithelium had taken up DQ OVA (Fig. 3*A*, 3*B*), as had the M cells located in the NALT epithelium (Fig. 3*C*). Recombinant *Salmonella*-GFP was also observed in M cells in the single layer of nasal epithelium after intranasal administration (Fig. 4*A*, 4*B*). These findings demonstrate that, like NALT M cells (Figs. 3*C*, 4*C*), respiratory M cells were capable of taking up both soluble protein and bacterial Ags.

To further demonstrate the biological significance of respiratory M cells, the numbers of these M cells per mouse were examined and compared with those of NALT M cells (Fig. 3*D*). The number of respiratory M cells was significantly higher than that of NALT M cells. Next, we examined the efficiency of Ag uptake per respiratory M cell and NALT M cell (Figs. 3*E–J*, 4*D–I*). Nasal passage and NALT epithelial cells isolated from BALB/c mice 30 min after intranasal instillation of DQ OVA or recombinant *Salmonella*-GFP were counterstained with PE–UEA-1 for flow cytometric analysis. The UEA-1$^+$ fraction showed a significantly greater efficiency of uptake of DQ OVA Ag and recombinant *Salmonella*-GFP than did UEA-1$^-$ cells isolated from the re-

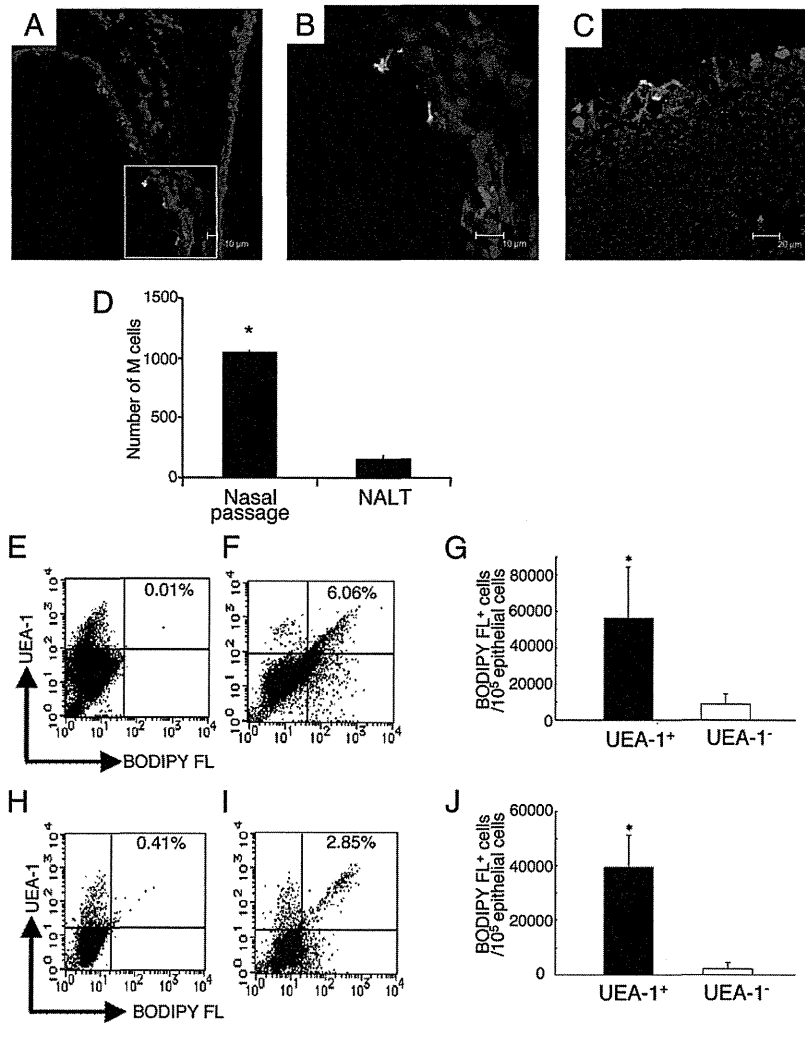

FIGURE 3. Respiratory M cells can take up DQ OVA. *A* and *B*, Immunofluorescence staining of nasal passages in BALB/c mice 30 min after DQ OVA (0.5 mg, green) instillation. Frozen sections of nasal passage were stained with rhodamine–UEA-1 (red) and DAPI (blue). Scale bars, 10 μm. The merged image is shown in *A*. An enlargement of the area in the rectangle in *A* is shown in *B*. These pictures demonstrate DQ OVA uptake by UEA-1^+ respiratory M cells. *C*, UEA-1^+ (red) NALT M cells in BALB/c mice also show an ability to take up DQ OVA (green). Scale bar, 20 μm. The results are representative of seven independent experiments. *D*, The numbers of UEA-1^+WGA$^-$ cells in nasal passages and NALT were quantified. The results are representative of four independent experiments. Flow cytometric analysis of DQ OVA uptake by UEA-1^+ respiratory (*E–G*) and NALT (*H–J*) M cells 30 min after intranasal instillation of PBS (*E*, *H*; control) or DQ OVA (*F*, *I*). *G* and *J*, UEA-1^+ cells showed significantly higher uptake of DQ OVA than did UEA-1^- cells in the nasal passages and NALT. The results are representative of four independent experiments. $*p < 0.05$.

spiratory epithelium of the nasal passage (Figs. 3*E–G*, 4*D–F*) and NALT (Figs. 3*H–J*, 4*G–I*).

Three-dimensional confocal microscopic analysis demonstrated that UEA-1^+ GFP$^+$ cells, which were sorted from the nasal passages of the mice intranasally infected with GFP-*Salmonella*, had captured and taken up the bacteria (Fig. 4*J*, Supplemental Video 1).

Cluster formation by respiratory M cells and DCs in response to inhaled respiratory pathogens

Because respiratory M cells are capable of capturing bacterial Ag, we considered it important to assess these cells as potential new entry sites for respiratory pathogens such as GAS. Confocal microscopic analysis demonstrated that, after its intranasal instillation, GAS stained with FITC–anti-*Streptococcus* A Ab was taken up by UEA-1^+ respiratory M cells (Fig. 5*B–E*). SEM analysis also revealed the presence of GAS-like microorganisms on the membranes of respiratory M cells after nasal challenge with GAS (Supplemental Fig. 2*A*). As one might expect, GAS were found in UEA-1^+ NALT M cells (Supplemental Fig. 2*B*) as well, confirming a previously reported result (20). Our findings suggest that respiratory M cells act as alternative entry sites for respiratory pathogens.

When we examined the site of invasion by GAS, we noted the presence of CD11c$^+$ DCs underneath the respiratory M cells (Fig. 5). Confocal microscopic analysis of the nasal passage epithelium after intranasal instillation of GAS revealed evidence of the recruitment of DCs, some having contact with the GAS, to the area underneath the respiratory M cells (Fig. 5*B–E*). A few DCs were also observed in the nasal passages of naive mice (Fig. 5*A*); these nasal DCs might preferentially migrate to the area underneath the respiratory M cells to receive Ags from these cells for the initiation of Ag-specific immune responses.

Presence of respiratory M cells in NALT-deficient mice

When we examined the numbers of respiratory M cells in the lymphoid structure-deficient Id$2^{-/-}$ mice (including NALT, NALT-null), the frequency of occurrence of respiratory M cells was comparable to that found in their littermate Id$2^{+/-}$ mice (Fig. 6*A*). This finding suggested that development of respiratory M cells occurred normally under NALT-null or Id2-deficient conditions. Frozen tissue samples were next prepared from NALT-null mice that had received fluorescence-labeled bacteria by intranasal instillation. Immunohistological analysis of these samples revealed the presence of recombinant *Salmonella*-GFP in UEA-1^+ cells from the nasal epithelium of Id$2^{-/-}$ mice. GFP-positive bacteria were also located in the subepithelial region of the nasal passages, suggesting that, in the NALT-null mice, some of the nasally deposited bacteria were taken up by respiratory M cells (Fig. 6*B*, 6*C*). Flow cytometric analysis confirmed the uptake of recombinant *Salmonella*-GFP by UEA-1^+ M cells, with UEA-1^+ cells in the nasal passages of Id$2^{-/-}$ mice showing a significantly higher uptake than UEA-1^- cells (Fig. 6*D–F*).

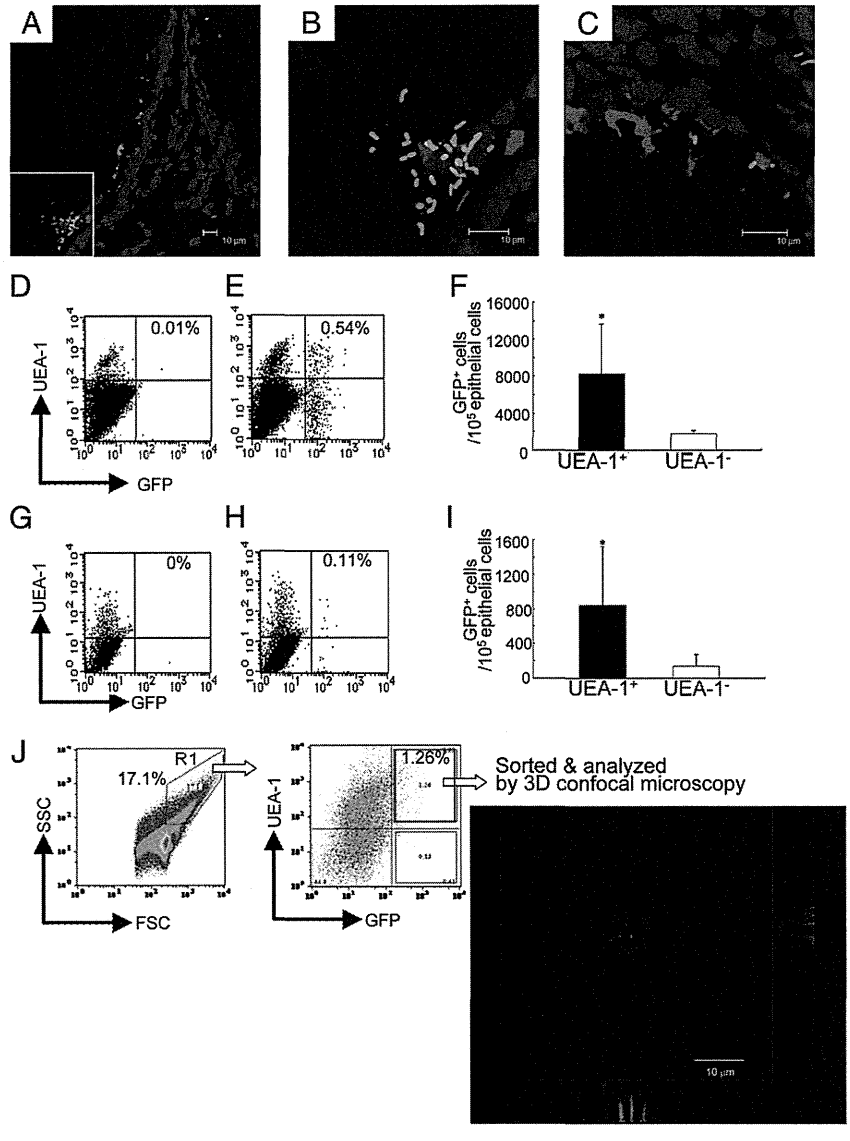

FIGURE 4. Respiratory M cells show an ability to take up recombinant *Salmonella*-GFP. *A* and *B*, Immunofluorescence staining of the nasal passages of BALB/c mice 30 min after GFP-*Salmonella* (5×10^8 CFU, green) instillation. Frozen sections of nasal passage were stained with rhodamine–UEA-1 (red) and DAPI (blue). The merged image is shown in *A*. An enlargement of the area in the rectangle in *A* is shown in *B*. These pictures demonstrate the ability of UEA-1^+ respiratory M cells, like UEA-1^+ NALT M cells (*C*), to take up GFP-*Salmonella*. The results are representative of six separate experiments. *A–C*, Scale bars, 10 μm. Flow cytometric analysis of GFP-*Salmonella* uptake by UEA-1^+ respiratory (*D–F*) and NALT (*G–I*) M cells 30 min after intranasal instillation of PBS (*D*, *G*; control) or GFP-*Salmonella* (*E*, *H*). *F* and *I*, Efficiency of uptake of GFP-*Salmonella* by UEA-1^+ cells in both nasal passages and NALT. The data showed UEA-1^+ M cells to be significantly more efficient than UEA-1^- epithelial cells at taking up GFP-*Salmonella*. The results are representative of five independent experiments. *J*, Three-dimensional confocal microscopic analysis demonstrated that UEA-1^+ GFP^+ cells, which were sorted from the nasal passages of mice intranasally infected with GFP-*Salmonella* (green), took up bacteria. Scale bar, 10 μm. The results are representative of three separate experiments. $^*p < 0.05$.

Induction of Ag-specific immune responses in NALT-deficient mice

NALT-null ($Id2^{-/-}$) mice and their littermate $Id2^{+/-}$ mice were intranasally immunized with recombinant *S. typhimurium* BRD 847 expressing a 50-kDa ToxC fragment of tetanus toxin (recombinant *Salmonella*-ToxC) to examine whether Ag sampling via respiratory M cells could induce Ag-specific immune responses in NALT-deficient mice. To eliminate any possible GALT-associated induction of Ag-specific immune responses from the swallowing of bacterial solutions after intranasal immunization, mice were given drinking water containing gentamicin from 1 wk before the immunization to the end of the experiment and were also subjected to intragastric lavage with 500 μl gentamicin solution before and after intranasal immunization. This protocol successfully eliminated the possibility of the intranasally delivered bacteria becoming deposition in the intestine (Supplemental Fig. 1). The titer of TT-specific serum IgG Ab was as high in $Id2^{-/-}$ mice as in $Id2^{+/-}$ mice (Fig. 6*G*). TT-specific IgA Abs were also detected in the nasal secretions and vaginal washes of intranasally immunized NALT-deficient mice (Fig. 6*H*, 6*I*). As expected, TT-specific Abs were not detected in either $Id2^{-/-}$ or $Id2^{+/-}$ mice intranasally immunized with a control recombinant *Salmonella* that did not express the ToxC gene (Fig. 6*G–I*). In addition to the responses to *Salmonella*, GAS-specific immune responses were induced in the absence of NALT in the experiment with $Id2^{-/-}$ mice (Fig. 6*J–L*). These data indicate that the respiratory M cell is an important Ag-sampling site for the induction of Ag-specific local IgA and serum IgG immune responses.

Discussion

In this study, we show the existence of a novel Ag sampling site for inhaled Ags in the upper respiratory epithelium. The murine nasal membrane has been reported to contain four types of epithelium: respiratory, olfactory, transitional, and squamous (21). Most of the respiratory epithelium is located in the lateral and ventral regions of the nasal cavity and is covered with pseudostratified ciliated columnar cells (21). In this study, we were also able to observe a single-layer epithelium on the lateral surfaces of the turbinates, which was comprised exclusively of UEA-$1^+$$WGA^-$ M cells (Fig. 1). These respiratory M cells showed specific reactivity to our previously developed M cell-specific mAb NKM 16-2-4 (12). Because NALT is characterized by follicle-associated epithelium, we first thought that this single-layer epithelium could represent the follicle-associated epithelium of the nasal passage. However,

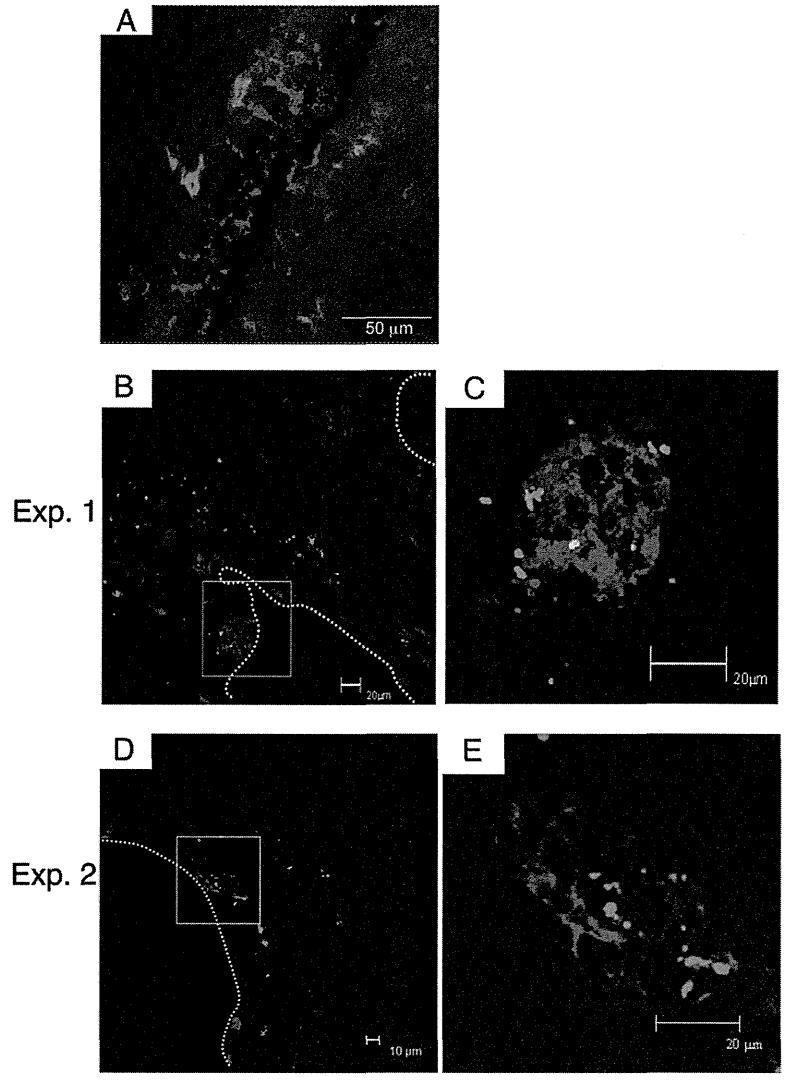

FIGURE 5. Respiratory M cells form clusters with DCs after GAS infection. *A*, Before nasal challenge with GAS, only a few DCs (FITC-CD11c$^+$, green) were associated with UEA-1$^+$ M cells (red) in the nasal passage. Scale bar, 50 μm. *B–E*, Two sets of confocal views of the nasal passage 5 d after intranasal instillation of GAS (Exp. 1 and Exp. 2, respectively). Frozen sections of the nasal passage were stained with FITC–anti-*Streptococcus* A Ab (green), rhodamine–UEA-1 (red), and allophycocyanin-CD11c (blue). These images reveal large numbers of DCs congregated underneath the UEA-1$^+$ respiratory M cells; some of the DCs were closely associated with GAS infiltrated through the UEA-1$^+$ respiratory M cells. *C* and *E* are enlargements of the areas in the squares shown in *B* and *D*, respectively. The results are representative of five independent experiments. *B*, *C*, and *E*, Scale bars, 20 μm; *D*, scale bar, 10 μm.

we ruled out this possibility when we could not find any organized lymphoid structures beneath the single-layer epithelium. The respiratory M cells had most of the classical features of M cells, including a depressed surface covered with short and irregular microvilli. However, TEM analysis revealed that, unlike NALT M cells, they lacked an intraepithelial pocket (Fig. 2). Examination of the numbers of respiratory and NALT M cells per nasal cavity revealed that there were more respiratory M cells than NALT M cells (in general six or seven times more; Fig. 3*D*), suggesting that the respiratory M cell plays a critical role as a gateway for the upper airway.

The anatomical and histological characteristics of the nasal cavity differ markedly between humans and mice. Reflecting this fact, the occurrence of single-layer epithelium also differs between the two species. Murine respiratory epithelium consists of a typical single-layer epithelium with traditional columnar epithelial cells in the turbinate portion of the nasal cavity, whereas pseudostratified columnar epithelium covers the olfactory epithelium (21, 22). In contrast, the traditional single-layer epithelium is not observed in the human nasal cavity, and both the upper respiratory surfaces and the olfactory surfaces are covered by pseudostratified columnar epithelium (23, 24). These differences suggest that the presence of respiratory M cells in the nasal cavity might be a feature unique to the mouse. The presence or absence of respiratory M cells in the human nasal cavity still needs to be carefully examined, and, if these cells are present, their contribution to the uptake of inhaled Ags needs to be investigated in future studies.

Previously, M cells in the lower respiratory tract were found to provide a portal of entry for bacterial pathogens into the lung (25). Our study suggests that the newly identified NALT-independent M cells in the upper respiratory tract provide an alternative portal of entry for nasally inhaled pathogens. The respiratory epithelium comprises three distinct Ag-sampling and/or pathogen-invasion sites: respiratory M cells and NALT M cells in the upper respiratory tract and M cells in the lower respiratory tract. It is interesting to speculate that the nature of the respiratory pathogen may dictate its preferred entry site, with GAS preferentially invading the host via the upper respiratory tract M cells and *Mycobacterium tuberculosis* preferentially invading via the lower respiratory tract M cells. This attractive possibility requires careful examination, and such a line of investigation has been initiated in our laboratory.

Salmonella, a known gastrointestinal pathogen, may have no relevance to the immunological and physiological aspects of Ag uptake by respiratory M cells. However, when used as a live vector for the intranasal delivery of vaccine Ags, attenuated *Salmonella* effectively elicits Ag-specific immune responses (26–29). Pasetti et al. (28) compared intranasal and orogastric immunizations in

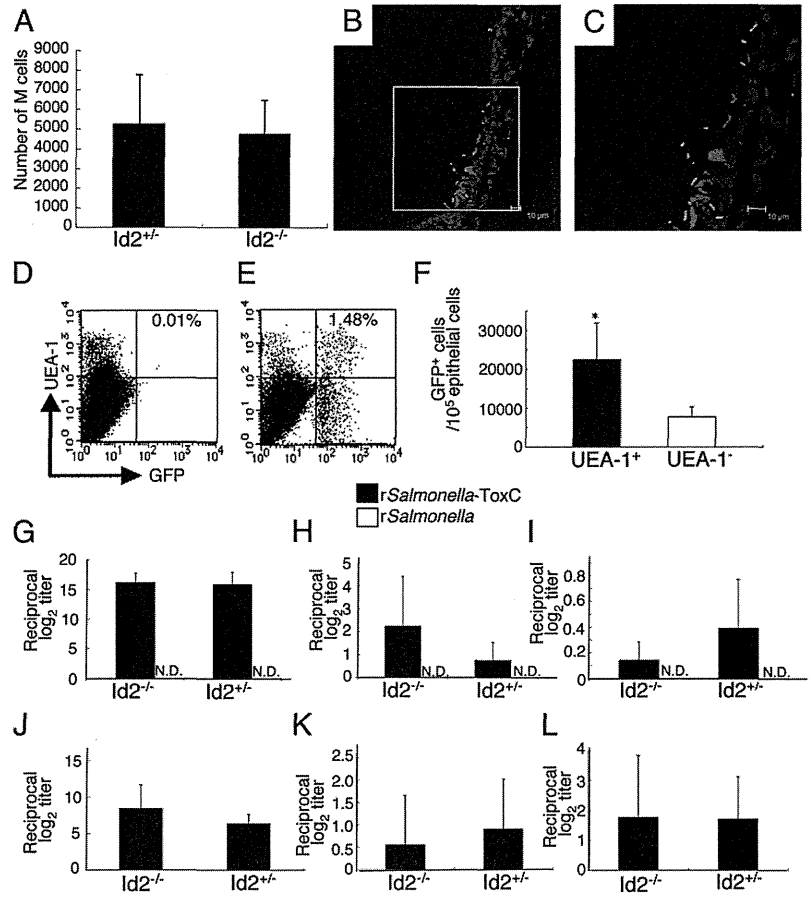

FIGURE 6. Id2$^{-/-}$ mice, which lack NALT, can take up GFP-*Salmonella*, which induce Ag-specific immune responses in UEA-1^{+} respiratory M cells. *A*, The numbers of UEA-1^{+}WGA^{-} cells in nasal passages of Id2$^{-/-}$ and Id2$^{+/-}$ mice were measured. The results are representative of four independent experiments. *B* and *C*, Immunofluorescence staining of nasal passages of Id2$^{-/-}$ mice in which GFP-expressing *Salmonella* (green) had been instilled. Frozen sections of nasal passages were stained with rhodamine–UEA-1 (red) and DAPI (blue). Scale bars, 10 μm. *C* is an enlargement of the area in the square shown in *B*. The results are representative of three independent experiments. *D–F*, Flow cytometric analysis of GFP-*Salmonella* uptake by UEA-1^{+} M cells 30 min after intranasal instillation of PBS (*D*; control) or GFP-*Salmonella* (*E*) in the nasal passages of Id2$^{-/-}$ mice. *F*, Efficiency of uptake by UEA-1^{+} cells in the nasal passages of Id2$^{-/-}$ mice was significantly greater than that by UEA-1^{-} cells. The results are representative of three independent experiments. *G–I*, NALT-deficient (Id2$^{-/-}$) mice and Id2$^{+/-}$ mice were intranasally immunized with recombinant *Salmonella*-ToxC (2.5×10^8 CFU) or recombinant *Salmonella* (2.5×10^8) alone three times at weekly intervals. They were given gentamicin-containing drinking water and also subjected to intragastric lavage with gentamicin solution to eliminate GALT-mediated Ag-specific immune responses. Samples were obtained 7 d after the last intranasal immunization to measure TT-specific Igs by ELISA. Serum IgG (*G*), nasal wash IgA (*H*), vaginal wash IgA (*I*). The results are representative of three independent experiments. *J–L*, As was the case with *Salmonella*, GAS-specific immune responses were induced in the absence of NALT (i.e., in Id2$^{-/-}$ mice), this time by a single intranasal injection of GAS (2×10^8 CFU). Serum IgG (*J*), nasal wash IgA (*K*), vaginal wash IgA (*L*). There were no statistical differences between Id2$^{-/-}$ and Id2$^{+/-}$ mice, as analyzed by the unpaired Mann–Whitney *U* test. The results are representative of five independent experiments. $^{*}p < 0.05$. N.D., not detected.

terms of both Ag-specific immune responses and in vivo distribution of vaccine organisms; they demonstrated that intranasal immunization resulted in greater humoral and cell-mediated immune responses and in the delivery of larger numbers of vaccine organisms to the nasal tissues, lungs, and Peyer's patches. Furthermore, intranasal immunization effectively induces Ag-specific IgA Abs in the reproductive secretions of mice and primates (30, 31). Notably, the levels of Ag-specific IgA Abs in the nasal secretions of NALT-deficient Id2$^{-/-}$ mice were not significantly higher than, or comparable to, those of control tissue-intact mice following intranasal immunization with recombinant *Salmonella* expressing ToxC (Fig. 6*H*) or GAS (Fig. 6*K*), respectively. In contrast, in intranasally immunized NALT-deficient mice, the levels of Ag-specific IgA Abs in remote secretions such as the vaginal wash were not significantly lower than, or comparable to, those in similarly treated tissue-intact mice (Fig. 6*I*, 6*L*). Inasmuch as these results revealed no significant differences between the two groups of intranasally immunized mice, our results at least suggest that respiratory M cells contribute to the induction of Ag-specific immune responses at both local and distant effector sites. However, we still need to carefully examine and compare the contributions of respiratory M cells and NALT M cells in the initiation of Ag-specific IgA Ab responses at local (e.g., airway) and distant (e.g., reproductive tract) effector sites.

In regard to the functional aspects of respiratory M cells, our data demonstrated that the numbers of respiratory M cells that took up OVA were comparable to those of NALT M cells (Fig. 3*G*, 3*J*). In contrast, 10 times more respiratory M cells than NALT M cells took up *Salmonella*; this result suggested that respiratory M cells are more efficient at taking up bacterial (or particulate) Ags than are NALT M cells (Fig. 4*F*, 4*I*). Although we do not have any data regarding the mechanism(s) behind these findings, these results

suggest that there may be functional differences in, for example, Ag uptake capability, between respiratory M cells and NALT M cells due to possible differences in the expression of bacterial Ag receptors, even though the morphologies and phenotypes of these two subsets of M cells are similar. In support of this possibility, it has been shown that the expression of a GP-2–specific receptor for FimH bacteria is restricted to Peyer's patches and not villous M cells; this situation may be analogous to that of NALT and respiratory M cells (32). Although the molecular mechanisms for the induction of Ag-specific immune responses by intranasal immunization and the efficacy of intranasal inoculation await elucidation, we demonstrated in this paper that respiratory M cells, like NALT M cells, are capable of sampling *Salmonella*, thereby opening a new avenue for the uptake of *Salmonella*-delivered vaccine.

CD18-expressing phagocytes (33) and mucosal DCs (34) are involved in the uptake of pathogens from the lumen of the intestine, but their role in the upper respiratory tract has never been clarified. Moreover, we found no evidence that mucosal DCs take up pathogens from the lumen of the nasal passage by expanding their dendrites into the lumen after nasal challenge with GAS. It was recently shown that intranasal immunization of mice with OVA plus adenovirus vector expressing Flt3 ligand as a mucosal adjuvant selectively increases $CD11b^+$ DC numbers in the nasal passages more effectively than those in NALT and subsequently induces Ag-specific Ab and CTL responses (35). Therefore, we speculated that the induction of immune responses in the murine model of intranasal administration of bacteria (e.g., *Salmonella* and GAS) might depend on the presence of appropriate initial Ag sampling sites associated with M cells, which can internalize the vaccine organisms. In this study, DCs were rarely detected in the subepithelial layer or the epithelial layer of the nasal passage in naive mice (Fig. 5*A*). It is important to note that DCs migrated to the area underneath the respiratory M cells and accumulated there to form cell clusters after exposure to respiratory pathogens (Fig. 5*B–D*). Following mucosal exposure to pathogens, submucosal DCs accumulate underneath infected mucosal epithelium that is not associated with organized lymphoid follicles (36, 37). Furthermore, these Ag-capturing DCs are capable of migrating into the draining lymph nodes (dLNs), where they encounter naive T cells for initial Ag-priming (36, 37). The question of whether DCs resident in the nasal passages migrate to the submucosal area to receive inhaled pathogens taken up via respiratory M cells and then travel to the dLNs (e.g., the cervical lymph nodes) to initiate an Ag-specific immune response remains to be addressed. It is interesting to postulate that respiratory M cells could be alternative airway Ag sampling sites for subsequent processing or presentation by nasal passage DCs, thereby initiating Ag-specific immune responses in the dLNs. In support of this hypothesis, it has been shown that Ag-specific Th cells are generated and found in the NALT and dLNs of mice given GAS intranasally (38). Our current study offers proof in support of this hypothesis by showing that *Salmonella* were effectively taken up by upper respiratory tract M cells in NALT and respiratory M cells and that a live vector-containing vaccine Ag induced Ag-specific immune responses via the nasal route.

We showed that TT-specific serum IgG and nasal wash IgA immune responses after intranasal immunization with recombinant *Salmonella*-ToxC were as high in $Id2^{-/-}$ mice as in $Id2^{+/-}$ mice (Fig. 6*G*, 6*H*) and that the frequency of occurrence of respiratory M cells in $Id2^{-/-}$ mice was comparable to that in their littermate $Id2^{+/-}$ mice (Fig. 6*A*). Generally, as discussed above, submucosal and dermal DCs have been shown to migrate to (or to be located in) the area just beneath infected epithelium and to then migrate into the dLNs after they have captured Ags. The DCs then present the peptides derived from these Ags to naive T cells, which subsequently undergo differentiation to Ag-specific effector T cells (36, 37). It has further been suggested that, rather than the DCs harboring Ag-derived peptides migrating to the systemic compartments, such as spleen and other secondary lymphoid tissues, the effector T cells generated in the dLNs after mucosal or vaginal Ag application migrate to these compartments and initiate Ag-specific immune responses (36).

If the cross-talk system between the airway mucosal and systemic immune compartments is similar to that between the reproductive mucosal and systemic immune compartments, it is unlikely that, in $Id2^{-/-}$ mice, the initiation of Ag-specific immune responses, including the presentation of Ags to naive T cells, occurs through migration of nasal DCs into the spleen after the capture of GAS-Ags by respiratory M cells and DCs. However, we cannot rule out this possibility, because it is possible that the nasal immune system, including the system by which Ags are taken up by respiratory M cells, offers distinct Ag-capture, -processing, and -presentation mechanisms via nasal DCs for the generation and migration of Ag-specific effector T cell and B cells. We have also found B-1 cell populations in the nasal passages (N. Tanaka, S. Fukuyama, T. Nagatake, K. Okada, M. Murata, K. Goda, D-Y. Kim, T. Nochi, S. Sato, J. Kunisawa, T. Kaisho, Y. Kurono, and H. Kiyono, manuscript in preparation), and it is possible that these cells may contribute to the induction of Ag-specific Ig responses without any help from $CD4^+$ T cells. At this stage, this is mere speculation, and the precise mechanism needs to be addressed in the future.

Taken together, these findings led us to conclude that respiratory M cells are effective alternative sampling sites for nasally inhaled bacterial Ags and thus play a key role in the induction of systemic and local mucosal immune responses.

Acknowledgments

We thank the staff of the Division of Mucosal Immunology, Institute of Medical Science and the University of Tokyo for technical advice and helpful discussions.

Disclosures

The authors have no financial conflicts of interest.

References

1. Kiyono, H., and S. Fukuyama. 2004. NALT- versus Peyer's-patch-mediated mucosal immunity. *Nat. Rev. Immunol.* 4: 699–710.
2. Yuki, Y., and H. Kiyono. 2003. New generation of mucosal adjuvants for the induction of protective immunity. *Rev. Med. Virol.* 13: 293–310.
3. Fukuyama, S., T. Hiroi, Y. Yokota, P. D. Rennert, M. Yanagita, N. Kinoshita, S. Terawaki, T. Shikina, M. Yamamoto, Y. Kurono, and H. Kiyono. 2002. Initiation of NALT organogenesis is independent of the IL-7R, LTbetaR, and NIK signaling pathways but requires the Id2 gene and CD3(-)CD4(+)CD45(+) cells. *Immunity* 17: 31–40.
4. Hiroi, T., K. Iwatani, H. Iijima, S. Kodama, M. Yanagita, and H. Kiyono. 1998. Nasal immune system: distinctive Th0 and Th1/Th2 type environments in murine nasal-associated lymphoid tissues and nasal passage, respectively. *Eur. J. Immunol.* 28: 3346–3353.
5. Shikina, T., T. Hiroi, K. Iwatani, M. H. Jang, S. Fukuyama, M. Tamura, T. Kubo, H. Ishikawa, and H. Kiyono. 2004. IgA class switch occurs in the organized nasopharynx- and gut-associated lymphoid tissue, but not in the diffuse lamina propria of airways and gut. *J. Immunol.* 172: 6259–6264.
6. Shimoda, M., T. Nakamura, Y. Takahashi, H. Asanuma, S. Tamura, T. Kurata, T. Mizuochi, N. Azuma, C. Kanno, and T. Takemori. 2001. Isotype-specific selection of high affinity memory B cells in nasal-associated lymphoid tissue. *J. Exp. Med.* 194: 1597–1607.
7. Debertin, A. S., T. Tschernig, H. Tönjes, W. J. Kleemann, H. D. Tröger, and R. Pabst. 2003. Nasal-associated lymphoid tissue (NALT): frequency and localization in young children. *Clin. Exp. Immunol.* 134: 503–507.
8. Wiley, J. A., M. P. Tighe, and A. G. Harmsen. 2005. Upper respiratory tract resistance to influenza infection is not prevented by the absence of either nasal-associated lymphoid tissue or cervical lymph nodes. *J. Immunol.* 175: 3186–3196.

9. Lund, F. E., S. Partida-Sánchez, B. O. Lee, K. L. Kusser, L. Hartson, R. J. Hogan, D. L. Woodland, and T. D. Randall. 2002. Lymphotoxin-alpha-deficient mice make delayed, but effective, T and B cell responses to influenza. *J. Immunol.* 169: 5236–5243.
10. Rangel-Moreno, J., J. Moyron-Quiroz, K. Kusser, L. Hartson, H. Nakano, and T. D. Randall. 2005. Role of CXC chemokine ligand 13, CC chemokine ligand (CCL) 19, and CCL21 in the organization and function of nasal-associated lymphoid tissue. *J. Immunol.* 175: 4904–4913.
11. Yokota, Y., A. Mansouri, S. Mori, S. Sugawara, S. Adachi, S. Nishikawa, and P. Gruss. 1999. Development of peripheral lymphoid organs and natural killer cells depends on the helix-loop-helix inhibitor Id2. *Nature* 397: 702–706.
12. Nochi, T., Y. Yuki, A. Matsumura, M. Mejima, K. Terahara, D. Y. Kim, S. Fukuyama, K. Iwatsuki-Horimoto, Y. Kawaoka, T. Kohda, et al. 2007. A novel M cell-specific carbohydrate-targeted mucosal vaccine effectively induces antigen-specific immune responses. *J. Exp. Med.* 204: 2789–2796.
13. Jang, M. H., M. N. Kweon, K. Iwatani, M. Yamamoto, K. Terahara, C. Sasakawa, T. Suzuki, T. Nochi, Y. Yokota, P. D. Rennert, et al. 2004. Intestinal villous M cells: an antigen entry site in the mucosal epithelium. *Proc. Natl. Acad. Sci. USA* 101: 6110–6115.
14. Hopkins, S. A., F. Niedergang, I. E. Corthesy-Theulaz, and J. P. Kraehenbuhl. 2000. A recombinant *Salmonella typhimurium* vaccine strain is taken up and survives within murine Peyer's patch dendritic cells. *Cell. Microbiol.* 2: 59–68.
15. Niedergang, F., J. C. Sirard, C. T. Blanc, and J. P. Kraehenbuhl. 2000. Entry and survival of *Salmonella typhimurium* in dendritic cells and presentation of recombinant antigens do not require macrophage-specific virulence factors. *Proc. Natl. Acad. Sci. USA* 97: 14650–14655.
16. Chatfield, S. N., I. G. Charles, A. J. Makoff, M. D. Oxer, G. Dougan, D. Pickard, D. Slater, and N. F. Fairweather. 1992. Use of the nirB promoter to direct the stable expression of heterologous antigens in *Salmonella* oral vaccine strains: development of a single-dose oral tetanus vaccine. *Biotechnology (N. Y.)* 10: 888–892.
17. Yamamoto, M., P. Rennert, J. R. McGhee, M. N. Kweon, S. Yamamoto, T. Dohi, S. Otake, H. Bluethmann, K. Fujihashi, and H. Kiyono. 2000. Alternate mucosal immune system: organized Peyer's patches are not required for IgA responses in the gastrointestinal tract. *J. Immunol.* 164: 5184–5191.
18. Todome, Y., H. Ohkuni, K. Yokomuro, Y. Kimura, S. Hamada, K. H. Johnston, and J. B. Zabriskie. 1988. Enzyme-linked immunosorbent assay of antibody to group A *Streptococcus*-specific C carbohydrate with trypsin-pronase-treated whole cells as antigen. *J. Clin. Microbiol.* 26: 464–470.
19. Matulionis, D. H., and H. F. Parks. 1973. Ultrastructural morphology of the normal nasal respiratory epithelium of the mouse. *Anat. Rec.* 176: 64–83.
20. Park, H. S., K. P. Francis, J. Yu, and P. P. Cleary. 2003. Membranous cells in nasal-associated lymphoid tissue: a portal of entry for the respiratory mucosal pathogen group A *streptococcus. J. Immunol.* 171: 2532–2537.
21. Mery, S., E. A. Gross, D. R. Joyner, M. Godo, and K. T. Morgan. 1994. Nasal diagrams: a tool for recording the distribution of nasal lesions in rats and mice. *Toxicol. Pathol.* 22: 353–372.
22. Adams, D. R. 1972. Olfactory and non-olfactory epithelia in the nasal cavity of the mouse, Peromyscus. *Am. J. Anat.* 133: 37–49.
23. Cagici, C. A., G. Karabay, C. Yilmazer, S. Gencay, and O. Cakmak. 2005. Electron microscopy findings in the nasal mucosa of a patient with stenosis of the nasal vestibule. *Int. J. Pediatr. Otorhinolaryngol.* 69: 399–405.
24. Jafek, B. W., B. Murrow, R. Michaels, D. Restrepo, and M. Linschoten. 2002. Biopsies of human olfactory epithelium. *Chem. Senses* 27: 623–628.
25. Teitelbaum, R., W. Schubert, L. Gunther, Y. Kress, F. Macaluso, J. W. Pollard, D. N. McMurray, and B. R. Bloom. 1999. The M cell as a portal of entry to the lung for the bacterial pathogen *Mycobacterium tuberculosis. Immunity* 10: 641–650.
26. Galen, J. E., O. G. Gomez-Duarte, G. A. Losonsky, J. L. Halpern, C. S. Lauderbaugh, S. Kaintuck, M. K. Reymann, and M. M. Levine. 1997. A murine model of intranasal immunization to assess the immunogenicity of attenuated *Salmonella typhi* live vector vaccines in stimulating serum antibody responses to expressed foreign antigens. *Vaccine* 15: 700–708.
27. Locht, C. 2000. Live bacterial vectors for intranasal delivery of protective antigens. *Pharm. Sci. Technol. Today* 3: 121–128.
28. Pasetti, M. F., T. E. Pickett, M. M. Levine, and M. B. Sztein. 2000. A comparison of immunogenicity and in vivo distribution of *Salmonella enterica* serovar *Typhi* and *Typhimurium* live vector vaccines delivered by mucosal routes in the murine model. *Vaccine* 18: 3208–3213.
29. Pasetti, M. F., R. Salerno-Gonçalves, and M. B. Sztein. 2002. *Salmonella enterica* serovar *Typhi* live vector vaccines delivered intranasally elicit regional and systemic specific CD8+ major histocompatibility class I-restricted cytotoxic T lymphocytes. *Infect. Immun.* 70: 4009–4018.
30. Sakaue, G., T. Hiroi, Y. Nakagawa, K. Someya, K. Iwatani, Y. Sawa, H. Takahashi, M. Honda, J. Kunisawa, and H. Kiyono. 2003. HIV mucosal vaccine: nasal immunization with gp160-encapsulated hemagglutinating virus of Japan-liposome induces antigen-specific CTLs and neutralizing antibody responses. *J. Immunol.* 170: 495–502.
31. Imaoka, K., C. J. Miller, M. Kubota, M. B. McChesney, B. Lohman, M. Yamamoto, K. Fujihashi, K. Someya, M. Honda, J. R. McGhee, and H. Kiyono. 1998. Nasal immunization of nonhuman primates with simian immunodeficiency virus p55gag and cholera toxin adjuvant induces Th1/Th2 help for virus-specific immune responses in reproductive tissues. *J. Immunol.* 161: 5952–5958.
32. Hase, K., K. Kawano, T. Nochi, G. S. Pontes, S. Fukuda, M. Ebisawa, K. Kadokura, T. Tobe, Y. Fujimura, S. Kawano, et al. 2009. Uptake through glycoprotein 2 of FimH(+) bacteria by M cells initiates mucosal immune response. *Nature* 462: 226–230.
33. Vazquez-Torres, A., J. Jones-Carson, A. J. Bäumler, S. Falkow, R. Valdivia, W. Brown, M. Le, R. Berggren, W. T. Parks, and F. C. Fang. 1999. Extraintestinal dissemination of *Salmonella* by CD18-expressing phagocytes. *Nature* 401: 804–808.
34. Rescigno, M., M. Urbano, B. Valzasina, M. Francolini, G. Rotta, R. Bonasio, F. Granucci, J. P. Kraehenbuhl, and P. Ricciardi-Castagnoli. 2001. Dendritic cells express tight junction proteins and penetrate gut epithelial monolayers to sample bacteria. *Nat. Immunol.* 2: 361–367.
35. Sekine, S., K. Kataoka, Y. Fukuyama, Y. Adachi, J. Davydova, M. Yamamoto, R. Kobayashi, K. Fujihashi, H. Suzuki, D. T. Curiel, et al. 2008. A novel adenovirus expressing Flt3 ligand enhances mucosal immunity by inducing mature nasopharyngeal-associated lymphoreticular tissue dendritic cell migration. *J. Immunol.* 180: 8126–8134.
36. Zhao, X., E. Deak, K. Soderberg, M. Linehan, D. Spezzano, J. Zhu, D. M. Knipe, and A. Iwasaki. 2003. Vaginal submucosal dendritic cells, but not Langerhans cells, induce protective Th1 responses to herpes simplex virus-2. *J. Exp. Med.* 197: 153–162.
37. Allan, R. S., C. M. Smith, G. T. Belz, A. L. van Lint, L. M. Wakim, W. R. Heath, and F. R. Carbone. 2003. Epidermal viral immunity induced by CD8α^+ dendritic cells but not by Langerhans cells. *Science* 301: 1925–1928.
38. Park, H. S., M. Costalonga, R. L. Reinhardt, P. E. Dombek, M. K. Jenkins, and P. P. Cleary. 2004. Primary induction of CD4 T cell responses in nasal associated lymphoid tissue during group A streptococcal infection. *Eur. J. Immunol.* 34: 2843–2853.

Membrane-bound human SCF/KL promotes in vivo human hematopoietic engraftment and myeloid differentiation

Shinsuke Takagi,[1-3] Yoriko Saito,[1] Atsushi Hijikata,[4] Satoshi Tanaka,[1,5,6] Takashi Watanabe,[4] Takanori Hasegawa,[7] Shinobu Mochizuki,[7] Jun Kunisawa,[5] Hiroshi Kiyono,[5] Haruhiko Koseki,[7] Osamu Ohara,[4,8] Takashi Saito,[3,9] Shuichi Taniguchi,[2] Leonard D. Shultz,[10] and Fumihiko Ishikawa[1]

[1]Research Unit for Human Disease Models, RIKEN Research Center for Allergy and Immunology, Yokohama, Japan; [2]Department of Hematology, Toranomon Hospital, Tokyo, Japan; [3]Department of Immune Regulation Research, Chiba University of Medical and Pharmaceutical Sciences, Chiba, Japan; [4]Laboratory for Immunogenomics, RIKEN Research Center for Allergy and Immunology, Yokohama, Japan; [5]Division of Mucosal Immunology, Institute of Medical Science, University of Tokyo, Tokyo, Japan; [6]Nippon Becton Dickinson Company, Tokyo, Japan; [7]Laboratory for Developmental Genetics, RIKEN Research Center for Allergy and Immunology, Yokohama, Japan; [8]Department of Human Gene Research, Kazusa DNA Research Institute, Kisarazu, Japan; [9]Laboratory for Cell Signaling, RIKEN Research Center for Allergy and Immunology, Yokohama, Japan; and [10]The Jackson Laboratory, Bar Harbor, ME

In recent years, advances in the humanized mouse system have led to significantly increased levels of human hematopoietic stem cell (HSC) engraftment. The remaining limitations in human HSC engraftment and function include lymphoid-skewed differentiation and inefficient myeloid development in the recipients. Limited human HSC function may partially be attributed to the inability of the host mouse microenvironment to provide sufficient support to human hematopoiesis. To address this problem, we created membrane-bound human stem cell factor (SCF)/KIT ligand (KL)–expressing NOD/SCID/IL2rgKO (hSCF Tg NSG) mice. hSCF Tg NSG recipients of human HSCs showed higher levels of both human CD45$^+$ cell engraftment and human CD45$^+$CD33$^+$ myeloid development compared with NSG recipients. Expression of hSCF/hKL accelerated the differentiation of the human granulocyte lineage cells in the recipient bone marrow. Human mast cells were identified in bone marrow, spleen, and gastrointestinal tissues of the hSCF Tg NSG recipients. This novel in vivo humanized mouse model demonstrates the essential role of membrane-bound hSCF in human myeloid development. Moreover, the hSCF Tg NSG humanized recipients may facilitate investigation of in vivo differentiation, migration, function, and pathology of human mast cells. (*Blood*. 2012;119(12): 2768-2777)

Introduction

The humanized mouse system, a xenogeneic transplantation and engraftment model for human hematopoietic stem cells (HSCs) and peripheral blood (PB) mononuclear cells (MNCs), facilitates the investigation of human hematopoietic and immune systems in vivo.[1,2] Since the pioneering work using SCID-hu[3] and Hu-PBL-SCID models,[4] investigators have attempted to better recapitulate human biology in mice across xenogeneic immunologic barriers. Recently, the introduction of targeted null mutations of immune-related genes, such as *Rag1, Rag2, Il2rg*, or *Prf1* in recipient mice, has improved engraftment levels of human CD45$^+$ leukocytes.[2,5-9] However, limitations remain in the ability of the host mouse hematopoietic microenvironment to support human hematopoiesis. The impaired development of human T-lymphoid and myeloid lineage cells compared with human B-lymphoid lineage cells in NOD/SCID and other immune-compromised mice may be the result of the lack of appropriate microenvironmental support. The recently created human leukocyte antigen (HLA) class I expressing immune-compromised NOD/SCID/IL2r γ null (NSG) mice partially addresses this issue for human T-cell development. Human CD8$^+$ T cells developing within these recipients of transplanted human HSCs exhibited cytokine production and cytotoxicity in an HLA-restricted manner.[10-12]

To create a hematopoietic microenvironment more suitable for human myeloid development, we developed a new immune-compromised mouse strain that expresses human membrane bound stem cell factor (SCF) under the control of the phosphoglycerate kinase (PGK) promoter (hSCF Tg NSG). Using hSCF Tg NSG mice as recipients of human HSCs, we aimed to clarify the role of membrane-bound form of SCF in supporting the engraftment of human hematopoietic cells and influencing the differentiation of the human myeloid lineage in the recipient mouse BM, spleen, and other organs. Here we show nearly complete human hematopoietic chimerism in the BM of hSCF Tg NSG recipients. In the BM of these recipients, human granulocytes accounted for the majority of engrafted human cells reflecting the physiologic human BM status. In addition to the development of immature and mature granulocytes, c-Kit$^+$ human mast cells differentiated efficiently in BM, spleen, and mucosal tissues. The hSCF Tg NSG mice, by supporting efficient human myeloid development including mast cells, may serve as a novel platform for in vivo investigation of human mast cell development and allergic responses.

Methods

Mice

NOD.Cg-*Prkdc*^{scid} *IL2rg*^{tm1Wjl} (NSG) mice and NOD.Cg-*Prkdc*^{scid} *IL2rg*^{tm1Wjl} Tg(PGK1-KITLG*220)441Daw/J, abbreviated as hSCF Tg NSG mice,

Submitted May 6, 2011; accepted October 2, 2011. Prepublished online as *Blood* First Edition paper, January 25, 2012; DOI 10.1182/blood-2011-05-353201.

The online version of this article contains a data supplement.

The publication costs of this article were defrayed in part by page charge payment. Therefore, and solely to indicate this fact, this article is hereby marked "advertisement" in accordance with 18 USC section 1734.

were generated at The Jackson Laboratory. The human membrane-bound SCF transgene driven by the human PGK promoter was backcrossed more than 10 generations from the original C3H/HeJ strain background[13] onto the NSG strain. All the mice were bred and maintained at The Jackson Laboratory and animal facility at RIKEN RCAI under defined flora according to guidelines established and approved by the Institutional Animal Committees at each respective institution.

Purification and transplantation of human HSCs

All experiments were performed with authorization from the Institutional Review Board for Human Research at RIKEN RCAI. Cord blood (CB) samples were first processed for isolation of MNCs using LSM lymphocyte separation medium (MP Biomedicals). CB MNCs were then enriched for human $CD34^+$ cells using anti–human CD34 microbeads (Miltenyi Biotec) and sorted for 7-AAD^- lineage ($hCD3/hCD4/hCD8/hCD19/hCD56)^-CD34^+CD38^-$ HSCs using FACSAria (BD Biosciences). To achieve high purity of donor HSCs, doublets were excluded by analysis of forward scatter (FSC)–height/FSC-width and side scatter (SSC)-height/SSC-width. Purity of each sorted sample was higher than 95%. Newborn (within 2 days of birth) hSCF Tg and non-Tg NSG recipients received 150 cGy total body irradiation using a ^{137}Cs-source irradiator, followed by intravenous injection of 5×10^2 to 5.3×10^4 sorted HSCs via the facial vein.

Analysis of human cell engraftment by flow cytometry

The recipient PB harvested from the retro-orbital plexus was evaluated for human hematopoietic engraftment every 3 to 4 weeks starting at 4 to 6 weeks after transplantation. After lysis of erythrocytes, cells were stained with anti-hCD45, anti-msCD45, anti-hCD3, anti-hCD19, anti-hCD33, and anti-hCD56 to determine human hematopoietic chimerism and to analyze cell lineages engrafted in the recipients. At 8 to 35 weeks after transplantation, the recipients were killed and single-cell suspensions of BM and spleen were analyzed using flow cytometry. Antibodies used for flow cytometry are specified in supplemental Methods (available on the *Blood* Web site; see the Supplemental Materials link at the top of the online article). The labeled cells were analyzed using FACSCantoII or FACSAria (BD Biosciences).

Morphologic analysis of cytospin specimens

Cytospin specimens of FACS-purified human myeloid cells were prepared with a Shandon Cytospin 4 cytocentrifuge (Thermo Electric) using standard procedures. To identify nuclear and cytoplasmic characteristics of each myeloid cell, cytospin specimens were stained with 100% May-Grünwald solution (Merck) for 3 minutes, followed by 50% May-Grünwald solution in phosphate buffer (Merck) for additional 5 minutes, and then with 5% Giemsa solution (Merck) in phosphate buffer for 15 minutes. All staining procedures were performed at room temperature. Light microscopy was performed with Zeiss Axiovert 200 (Carl Zeiss).

Microarray analysis

Purified $hCD45^+CD33^+c\text{-}Kit^-CD203c^-HLA\text{-}DR^-$ granulocytes and $hCD45^+CD33^+$ $c\text{-}Kit^-CD203c^-HLA\text{-}DR^+CD14^+$ monocytes from BM of 4 hSCF Tg NSG recipients and 3 non-Tg NSG recipients as well as neutrophils and monocytes from 2 healthy persons were evaluated using Human Genome U133 plus Version 2.0 GeneChips (Affymetrix). Total RNA was extracted with TRIzol (Invitrogen) from more than 10^4 sorted cells and amplified to cDNA using the Ovation Pico WTA System (Nugen). Biotinylated cDNA was synthesized with Two-Cycle Target Labeling Kit (Affymetrix). Microarray data were analyzed using the Bioconductor package (Bioconductor; http://www.bioconductor.org). The signal intensities of the probe sets were normalized using the GC-RMA program (Bioconductor). The RankProd program was used to select differentially expressed genes with a cutoff P value of less than .01 and an estimated false-positive rate of less than 0.05.[14] Gene annotation was obtained from Ingenuity Pathway Analysis and Gene Ontology Annotation databases (Ingenuity systems, http://www.ingenuity.com; Gene Ontology Annotation, http://www.ebi.ac.up/GOA). For differentially transcribed genes, GO term enrichment analysis was performed according to a method described by Draghici et al[15] with a correction of multiple testing using false discovery rate.[16] Eventually, GO terms with the false discovery rate-corrected P value $< .05$ were selected as functionally enriched terms. Raw data for microarray data are accessible at the RefDIC database (http://refdic.rcai.riken.jp) under the following accession numbers: RSM06616, RSM06617, RSM06618, RSM06620, RSM06621, RSM06622, RSM06623, RSM06633, RSM06642, RSM06648, RSM06665, RSM06667, RSM06668, RSM06669, RSM06670, RSM08241, and RSM08243. Differences in expression levels were considered significant if P is $< .05$ using Kruskal-Wallis, Wilcoxon-Mann-Whitney, or Student t test in KaleidaGraph (Synergy Software).

IHC and immunofluorescence imaging

Thin (~ 5-μm) sections prepared from paraformaldehyde-fixed paraffin-embedded tissues were stained with H&E using standard procedures. Immunohistochemistry (IHC) and immunofluorescence labeling were performed using standard procedures. Antibodies used for IHC and immunofluorescence labeling were mouse anti–human mast cell tryptase monocolonal antibody (Dako North America, clone AA1), mouse anti–human CD45 monoclonal antibody (Dako North America, clone $2B11^+PD7/26$), rabbit anti–human CD117 monoclonal antibody (Epitomics, clone YR145), and rabbit anti–human CD14 polyclonal antibody (Atlas Antibodies). Light microscopy was performed using an Axiovert 200 (Carl Zeiss). For quantification of $tryptase^+$ cell frequency, 3 high-power fields from 3 different recipients were examined using AutoMeasure module of AxioVision software (Release 4, Carl Zeiss). Confocal microscopy was performed using a LSM710 equipped with C-APOCHROMAT 40×/1.2 (Carl Zeiss).

Results

Human hematopoietic repopulation is enhanced in hSCF Tg NSG recipients

The humanized mouse model system has served as a tool to investigate human hematopoiesis, immunity, and diseases in vivo. However, one of the major limitations in the system is that the microenvironment supporting human hematopoiesis and immunity is primarily of mouse origin. In the present study, we created a strain of NSG mice expressing membrane-bound human SCF to analyze the role of the BM microenvironment in human hematopoietic lineage determination and development.

c-Kit, the receptor for SCF, is expressed at lower levels in human CB $Lin^-CD34^+CD38^-$ early HSCs and at high levels in mast cells.[17-19] For reconstitution of human myeloid and lymphoid cells, 5×10^2 to 5.3×10^4 FACS-purified CB $Lin^-CD34^+CD38^-$ HSCs were transplanted into newborn sublethally irradiated (1.5 Gy) hSCF Tg NSG mice and into non-Tg NSG controls (Table 1). To determine the kinetics of human hematopoietic chimerism in the recipient circulation, we performed flow cytometric analysis of PB every 3 to 4 weeks starting at 4 to 6 weeks after transplantation. During long-term observation, all the 21 hSCF Tg NSG recipient mice became moribund at 8 to 35 weeks after transplantation. Complete blood count analysis demonstrated reduced erythrocyte hemoglobin concentration in the PB of hSCF Tg NSG recipients compared with non-Tg NSG recipients (Figure 1A). Anemia in hSCF Tg NSG recipients was not associated with abnormalities in mean corpuscular volume, mean corpuscular hemoglobin, or mean corpuscular hemoglobin concentration (supplemental Figure 1). The suppression of host erythropoiesis in the hSCF Tg NSG recipients was related to the irradiation and engraftment of the human HSCs because unmanipulated nontransplanted hSCF Tg NSG mice did not develop anemia (supplemental Figure 1).

Table 1. Summary of hSCF Tg NSG and non-Tg NSG recipients analyzed

				CBC at time of death					% chimerism at time of death			% of CD45+ in BM				% of CD33+ in BM			% of CD45+ in BM			% chimerism of erythroid cells in BM
Recipient ID	CB ID	Graft dose	Survival, wks	WBC, × 10^3/L	RBC, × 10^4/μL	Hemoglobin, g/dL	Hematocrit, %	Platelets, ×10^3/μL	PB	BM	Spleen	CD33+	CD3+	CD19+	CD3−CD56+	CD117+CD203c+	HLA DR−	HLA DR+	CD117+CD203c+	HLA DR−	HLA DR+	
N1-1	1	5000	21	1.1	500	10.0	35.0	550	75.5	93.3	95.3	31.1	1.2	50.2	0.3	0.9	51.5	47.6	0.3	16.0	14.8	NA
N1-2	1	5000	16	1.4	730	13.0	44.0	1100	42.6	76.1	72.9	35.2	0.1	54.8	0.4	0.7	39.6	59.7	0.2	13.9	21.0	NA
N1-3	1	5000	24	NA	NA	NA	NA	NA	20.7	12.6	4.4	32.9	3.8	60.7	0.0	4.4	37.9	57.7	1.0	12.5	19.0	3.1
S1-1	1	5000	23	4.1	220	6.7	15.6	150	99.1	99.7	94.4	77.2	24.5	19.2	0.5	3.9	80.6	15.5	3.0	62.2	11.9	NA
S1-2	1	5000	20	6.8	220	5.0	18.0	30	83.2	99.4	97.7	75.5	2.6	28.4	0.3	6.7	68.7	24.6	5.1	51.8	18.6	36.3
S1-3	1	5000	21	0.7	320	7.0	25.0	330	76.9	99.7	95.8	70.9	1.5	16.6	0.2	14.6	50.0	35.4	10.4	35.5	25.1	0.0
S1-4	1	500	26	0.5	150	3.0	11.0	250	30.7	97.0	86.3	69.0	2.0	47.5	0.1	6.9	68.6	24.5	4.8	47.3	16.9	NA
N2-1	2	10 000	35	0.8	390	8.0	30.0	110	31.7	54.9	87.1	50.3	21.8	25.8	2.4	19.1	7.4	73.5	9.6	3.7	37.0	11.5
S2-1	2	10 000	16	1.3	186	4.1	13.2	583	90.7	96.6	99.3	18.7	3.2	40.6	1.2	34.4	18.0	47.6	6.4	3.4	8.9	NA
S3-1	3	10 000	13	0.2	215	3.9	12.6	793	52.0	97.8	90.9	54.2	0.0	42.8	0.7	19.0	44.6	36.4	10.3	24.2	19.7	NA
S3-2	3	10 000	15	2.2	161	3.1	9.8	458	93.6	99.6	98.2	61.5	4.4	20.4	1.4	7.3	60.5	32.2	4.5	37.2	19.8	NA
S4-1	4	10 000	13	0.5	97	1.9	5.1	6	98.6	100.0	98.2	52.0	1.2	39.8	0.3	2.7	81.9	15.4	1.4	42.6	8.0	27.2
N5-1	5	12 000	35	3.1	310	7.0	25.0	550	6.8	36.8	48.9	29.9	17.5	41.9	NA	22.6	7.0	70.4	6.8	2.1	21.1	5.8
N6-1	6	14 000	23	2.1	520	10.0	34.0	620	57.6	65.0	83.6	29.3	17.6	43.1	1.6	3.3	45.1	51.6	1.0	13.2	15.1	7.4
N6-2	6	14 000	21	1.6	680	12.0	40.0	660	64.6	25.3	81.5	10.4	17.2	64.4	0.5	33.9	17.5	48.6	3.5	1.8	5.1	1.4
N6-3	6	14 000	24	2.3	490	10.0	33.0	80	73.8	71.8	92.8	18.5	13.9	51.1	0.8	10.6	8.5	81.4	2.0	1.6	15.1	12.8
S6-1	6	14 000	16	2.2	236	4.5	15.5	33	70.0	88.5	94.7	39.4	5.8	43.6	0.7	68.9	8.1	23.0	27.1	3.2	9.1	33.1
S6-2	6	14 000	14	4.6	270	6.0	21.0	108	85.4	90.0	95.2	33.3	11.6	46.8	0.9	36.5	16.0	47.5	12.2	5.3	15.8	5.8
S7-1	7	15 000	16	4.9	293	6.1	19.4	132	93.6	99.7	98.8	76.5	1.4	42.3	0.6	1.6	80.1	18.3	1.2	61.3	14.0	NA
S8-1	8	16 000	13	1.0	183	3.3	9.4	78	98.6	100.0	99.7	16.2	19.9	52.1	0.9	25.1	1.0	73.9	4.1	0.2	12.0	NA
S8-2	8	16 000	11	1.0	376	5.6	18.4	568	89.5	99.6	98.5	48.6	0.2	54.5	0.6	4.9	42.0	53.1	2.4	20.4	25.8	NA
N9-1	9	18 000	20	2.7	650	13.0	42.0	130	71.6	87.2	92.0	15.0	1.7	72.4	0.4	1.4	24.7	74.0	0.2	3.7	11.1	9.8
S9-1	9	18 000	16	1.4	164	3.4	10.6	80	90.4	99.9	97.0	51.4	0.2	35.1	0.2	2.4	54.9	42.7	1.2	28.2	21.9	25.5
N10-1	10	20 000	19	1.0	660	12.0	42.0	77	38.4	46.5	87.1	25.9	44.4	24.1	0.8	3.9	6.2	89.9	1.0	1.6	23.3	12.0
N10-2	10	20 000	14	NA	NA	NA	NA	NA	NA	NA	NA	NA	NA	NA	NA	NA	NA	NA	NA	NA	NA	NA
N10-3	10	20 000	12	NA	NA	NA	NA	NA	NA	NA	NA	NA	NA	NA	NA	NA	NA	NA	NA	NA	NA	NA
S10-1	10	20 000	19	2.5	292	6.1	20.9	6	95.5	99.7	97.3	42.3	14.4	35.5	0.9	5.7	28.8	65.5	2.4	12.2	27.7	4.3
S10-2	10	20 000	14	1.5	170	3.0	11.0	30	95.8	99.7	89.3	27.3	28.4	28.0	5.4	18.6	19.8	61.6	5.1	5.4	16.8	17.1
N11-1	11	36 000	20	25.1	470	9.0	31.0	240	84.1	70.7	94.0	19.5	5.9	63.6	0.7	3.8	17.8	78.4	0.7	3.5	15.3	42.3
S11-1	11	36 000	10	19.2	420	8.0	27.0	410	77.5	98.0	95.3	34.0	0.2	43.5	0.5	4.5	34.6	60.9	1.5	11.8	20.7	58.5
N12-1	12	53 000	8	NA	NA	NA	NA	NA	36.9	95.6	83.3	20.3	0.0	72.2	0.2	NA	NA	NA	NA	NA	NA	NA
S12-1	12	53 000	11	NA	NA	NA	NA	NA	100.0	100.0	99.9	43.5	6.5	39.1	1.5	NA	NA	NA	NA	NA	NA	NA
S12-2	12	53 000	8	NA	NA	NA	NA	NA	93.1	100.0	NA	65.6	0.2	13.2	NA	1.6	83.7	14.7	1.0	54.9	9.6	NA
S12-3	12	53 000	13	13.6	211	3.9	10.9	165	57.0	79.5	68.3	47.5	12.5	35.7	2.2	8.8	59.9	31.3	4.2	28.5	14.9	NA
N13-1	13	17 000	20	6.4	720	13.0	45.0	470	39.2	85.0	81.8	21.8	0.0	69.0	0.2	0.4	46.1	53.5	0.1	10.0	11.7	7.6
S13-1	13	17 000	20	2.8	290	7.0	27.0	510	74.9	93.7	94.5	38.1	6.0	47.8	0.4	26.6	31.3	42.1	10.1	11.9	16.0	48.4

A total of 21 human HSC-engrafted hSCFTg NSG (S) recipients and 15 human HSC-engrafted non-Tg NSG (N) recipients were created.
WBC indicates white blood cell count; RBC, red blood cell count; and NA, not applicable.

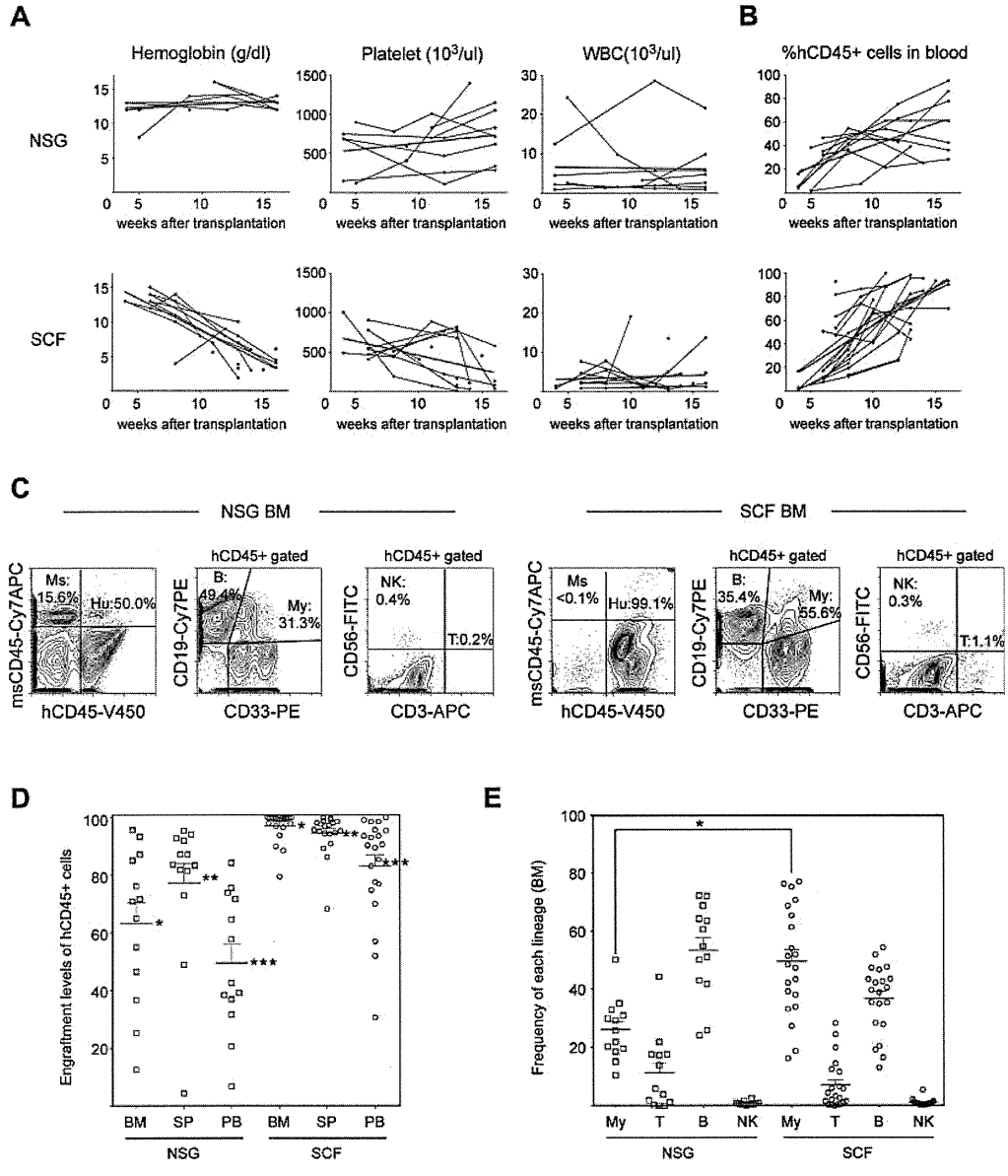

Figure 1. Human hematopoietic engraftment is enhanced in hSCF Tg NSG recipients. (A) hSCF Tg NSG recipients developed progressive anemia as evidenced by reduced hemoglobin concentration compared with non-Tg NSG mice transplanted with human HSCs from the same donor source. (B) Human CD45$^+$ chimerism was analyzed over time in PB of hSCF Tg and non-Tg NSG recipients. (C) Representative flow cytometric contour plots demonstrating the presence of human CD45$^+$ cells, CD19$^+$ B cells, CD33$^+$ myeloid cells, CD3$^+$ T cells, and CD56$^+$CD3$^-$ NK cells in recipient BM. (D) At the time of death, engraftment levels of human CD45$^+$ cells in the BM, spleen, and PB of hSCF Tg NSG recipients were significantly higher compared with non-Tg NSG controls (BM: hSCF Tg n = 21, non-Tg n = 13, $P < .0001$; spleen: hSCF Tg n = 21, non-Tg n = 13, $P = .0065$; PB: hSCF Tg n = 21, non-Tg n = 13, $P < .0001$). (E) In hSCF Tg NSG recipient BM, significantly greater human CD33$^+$ myeloid lineage development was observed (hSCF Tg n = 21, non-Tg n = 13, $P = .0002$).

Impaired mouse erythropoiesis in these engrafted hSCF Tg NSG mice was associated with rapid expansion of hCD45$^+$ hematopoietic cells compared with non-Tg NSG recipients (Figure 1B).

At 8 to 35 weeks after transplantation, individual hSCF Tg NSG recipients were analyzed to determine levels of reconstitution of human hematopoiesis and immunity in the BM, spleen, and PB. At the time of necropsy, we did not observe any gross macroscopic abnormalities in these recipients. We performed flow cytometric analysis to evaluate the engraftment levels of human CD45$^+$ cells (calculated as % hCD45$^+$ cells relative to total numbers of mouse and human CD45$^+$ cells in the nucleated cell gate). Engraftment levels of human CD45$^+$ leukocytes in the BM, spleen, and PB were significantly higher in hSCF Tg NSG recipients (mean ± SEM; 97.1% ± 1.1%, 94.5% ± 1.6%, and 83.1% ± 3.9%, respectively; n = 21) compared with engrafted non-Tg NSG recipients (63.1% ± 7.3%, 77.3% ± 6.9%, and 49.5% ± 6.5%, respectively; n = 13; $P < .0001$, $P = .0065$, and $P < .0001$ by 2-tailed t test, respectively; Figure 1C-D). Compared with enhanced engraftment of human leukocytes in the recipient BM, development of human erythroid precursors was not significantly different in hSCF Tg NSG recipients compared with non-Tg NSG recipients (hSCFTg: 25.6% ± 6.1%; n = 10 and non-Tg NSG controls: 11.4% ± 3.6%; n = 10; $P = .0601$; supplemental Figure 2). We next analyzed the development of human lymphoid and myeloid cells in the engrafted human CD45$^+$ hematopoietic cell populations by flow cytometry using monoclonal antibodies against hCD3, hCD19,

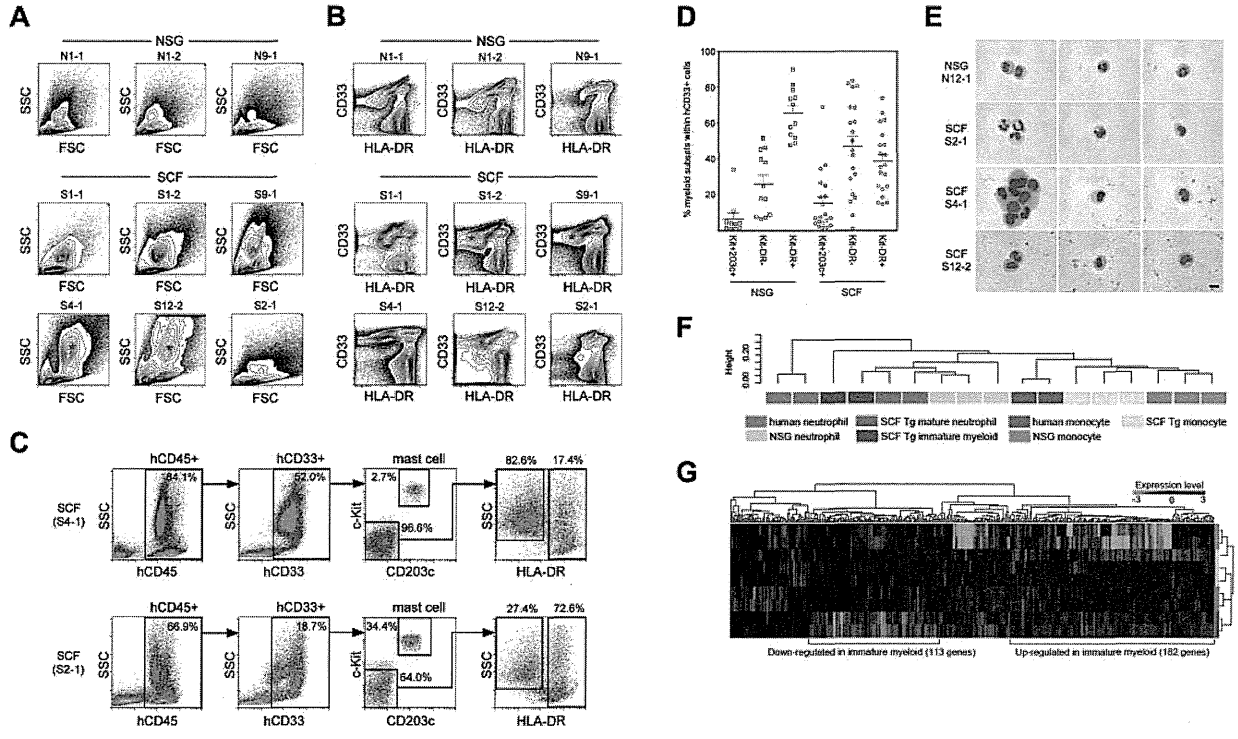

Figure 2. HLA-DR-negative human myeloid cells predominate in hSCF Tg NSG recipient BM. (A) Flow cytometric contour plots demonstrating FSC and SSC characteristics of 6 hSCF Tg NSG recipient BM (S1-1, S1-2, S9-1, S4-1, S12-2, and S2-1) and 3 non-Tg NSG recipient BM (N1-1, N1-2, and N9-1). Polymorphonuclear myeloid cells (red asterisks) are present at high frequencies in hSCF Tg NSG recipient BM. (B) Flow cytometry contour plots demonstrating hCD33 and HLA-DR expression in the same recipients as shown in panel A. Consistent with their FSC and SSC characteristics, hSCF Tg NSG recipient BM contained a prominent $CD33^+HLA\text{-}DR^-$ granulocyte population (red asterisks; N1-1, killed at 21 weeks; N1-2, killed at 16 weeks; N9-1, killed at 20 weeks; S1-1, killed at 23 weeks; S1-2, killed at 20 weeks; S9-1, killed at 16 weeks; S4-1, killed at 13 weeks; S12-2, killed at 8 weeks; and S2-1, killed at 16 weeks). (C) Representative flow cytometric scatter plots of hSCF Tg NSG recipient BM demonstrating the identification of human $c\text{-}Kit^+CD203c^+$ mast cells within the $hCD33^+$ fraction and $HLA\text{-}DR^-SSC^{high}$ granulocytes and $HLA\text{-}DR^+SSC^{low}$ APCs within the $c\text{-}Kit^-CD203c^-$ fraction (S4-1, killed at 13 weeks; and S2-1, killed at 16 weeks). (D) Frequencies of human $c\text{-}Kit^+CD203c^+$ mast cells, $CD33^+HLA\text{-}DR^-$ granulocytes, and $CD33^+HLA\text{-}DR^+$ APCs within the total $hCD45^+hCD33^+$ myeloid cell population in the BM of hSCF Tg and non-Tg NSG recipients. Numbers of cells in the granulocyte/neutrophil fraction were significantly higher in hSCF Tg NSG recipient BM (hSCF Tg n = 20, non-Tg n = 12, $P = .0001$). (E) $CD33^+HLA\text{-}DR^-$ cells from hSCF Tg and non-Tg NSG recipient BM were FACS-purified and examined by MGG staining. In 9 of 13 hSCF Tg recipients (S4-1 and S12-2 shown as representative), immature myeloid cells composed the majority of cells in this fraction. In 4 of 13 hSCF Tg recipients (S2-1 shown as representative) and 4 of 5 non-Tg NSG recipients (N12-1 shown as representative), mature neutrophils (band and segmented forms) were observed (N12-1, killed at 8 weeks; S2-1, killed at 16 weeks; S4-1, killed at 13 weeks; and S12-2, killed at 8 weeks). (F-G) Global transcriptional profiles of FACS-purified $CD33^+cKit^-CD203^-HLA\text{-}DR^-$ granulocytes and $CD33^+c\text{-}Kit^-CD203c^-HLA\text{-}DR^+CD14^+$ monocytes derived from hSCF Tg NSG and non-Tg NSG recipient BM as well as human $CD16^+$ neutrophils and $CD14^+$ monocytes were compared. (F) Unsupervised clustering for each group is shown. (G) The expression heatmap demonstrates genes that are significantly under- and over-represented in each population.

hCD56, and hCD33 along with anti–human and anti–mouse CD45 antibodies (Figure 1C,E). Although there was recipient-to-recipient variability, the frequency of human $CD33^+$ myeloid cells within the total human $CD45^+$ population was significantly higher in the hSCF Tg NSG recipient BM than in the non-Tg NSG recipient BM and constituted the majority of human hematopoietic cells (hSCF Tg: 49.7% ± 4.0%; n = 21 and non-Tg NSG controls: 26.2% ± 2.9%; n = 13; $P = .0002$ by 2-tailed t test). In contrast, in non-Tg NSG recipients, the majority of human hematopoietic cells in the BM were B cells (53.3% ± 4.5%; n = 13), consistent with previous reports.[5,9,20] These findings demonstrate that the expression of membrane-bound hSCF in BM microenvironment results in significantly more efficient engraftment of human HSCs as well as enhanced development of human $CD33^+$ myeloid cells from the engrafted human HSCs.

Human myeloid lineage development in hSCF Tg NSG recipients

Next, we examined the development of human myeloid subsets in the human membrane-bound SCF-expressing BM microenvironment. Flow cytometric scatter plots demonstrate the development of the SSC high granulocyte fraction in hSCF Tg NSG recipients, which correlate with $CD33^+HLA\text{-}DR^-$ cells (Figure 2A-B). To quantify the frequencies of different myeloid subsets in these recipients, we first identified $CD33^+c\text{-}Kit^+CD203c^+$ mature human mast cells among human $CD45^+$ cells. Next, we identified $CD33^+HLA\text{-}DR^-$ human granulocyte lineage cells and human $CD33^+HLA\text{-}DR^+$ antigen-presenting cells (APCs) among human $CD45^+$ cells excluding mature mast cells (Figure 2C).

In the hSCF Tg NSG recipient BM, there were increased percentages of $CD33^+HLA\text{-}DR^-$ granulocytes and decreased percentages of $CD33^+HLA\text{-}DR^+$ APCs compared with non-Tg NSG controls (hSCF Tg: 46.7% ± 5.9% and 38.3% ± 4.0%, respectively; n = 20 and non-Tg NSG controls: 25.8% ± 5.0% and 65.5% ± 4.1%, respectively; n = 12; $P = .0204$ and $P = .0001$ by 2-tailed t test, respectively; Figure 2D). In the BM of 11 of 20 hSCF Tg NSG recipients examined, $c\text{-}Kit^-CD203c^-HLA\text{-}DR^-$ SSC^{high} granulocytes accounted for the highest frequency of total human myeloid cells (Figure 2D; Table 1). To examine the morphologic features of the human granulocytes developing in the hSCF Tg recipients, we carried out May-Grünwald-Giemsa (MGG) staining using cytospin specimens of FACS-purified $CD33^+c\text{-}$